# Thermodynamics and Lattice Vibrations of Minerals:
# 1. Mineral Heat Capacities and Their Relationships to Simple Lattice Vibrational Models

Susan Werner Kieffer[1]

*Department of Earth and Space Sciences, University of California, Los Angeles, California 90024*

This is the first of a series of five papers in which the thermodynamic properties of minerals are interpreted in terms of lattice vibrational spectra. In this paper, measured heat capacities for minerals are examined in terms of the Debye theory of lattice vibrations, and it is demonstrated that heat capacities of silicates show large deviations from the behavior expected from Debye theory. The underlying assumptions of Debye theory are critically reviewed, and it is shown that the observed thermodynamic deviations in minerals probably arise from four effects not included in the Debye model: anisotropy of elastic parameters, dispersion of acoustic waves toward Brillouin zone boundaries, optic vibrations in excess of the Debye spectrum at low frequencies, and optic vibrations at frequencies much greater than the Debye cutoff frequency predicted by acoustic measurements. Each of the four effects influences the heat capacity in a particular temperature range: anisotropy, dispersion and low-frequency optic vibrations are important at low temperatures (0°K to ~100°K); high-frequency vibrations are important at higher temperatures. It is necessary to include all four effects in a generalized lattice vibrational model for minerals; such a model is developed in papers 2–5 of this series. The minerals included in this study are halite, periclase, brucite, corundum, spinel, quartz, cristobalite, silica glass, coesite, stishovite, rutile, albite, microcline, jadeite, diopside, enstatite, tremolite, talc, muscovite, forsterite, zircon, kyanite, andalusite, sillimanite, pyrope, grossular, andradite, spessartine, almandine and calcite.

## Contents

## 1. Introduction

Many geologic questions which are asked about properties of the earth and processes within it cannot be answered because of our lack of knowledge of properties of minerals. In some cases it is possible to measure the relevant properties on appropriate samples; for example, seismic velocities of crustal minerals and rocks can be measured by ultrasonic techniques, compressions of high-pressure phases can be measured by shock wave techniques, and phase equilibria at low pressure and temperature can be studied in laboratory experiments. In other cases, however, it is not possible to do the appropriate experiments, because, for example, pressures and temperatures of interest may not be attainable in the laboratory, samples may not be available, or equilibrium may not be attainable. Under such circumstances, geologists are forced to rely on empirical extrapolations of meager data or on theoretical methods.

Our current theories of the vibrational and thermodynamic behavior of minerals have been partially obtained by applying concepts developed for simple substances in the fields of physics, chemistry, and materials science. Frequently, the theories were originally developed to explain properties of substances whose characteristics differ sharply from those of minerals, e.g., for metals or for ionic solids. When they are applied to minerals, these theories may become artificial and, frequently, cumbersome because of the complexity of mineral structures.

Such has been the case with most attempts to apply lattice dynamics calculations to minerals. In the lattice dynamics approach, assumptions about the atomic force constants are made, and from these assumptions, elastic constants and their derivatives are calculated. The vibrational spectrum, which is required in order to calculate the thermodynamic functions, can be obtained from such models. In principle, the formalism of lattice dynamics provides great power to calculate mineral properties and to interrelate elastic constant, spectral, thermodynamic, and phase equilibrium data. In practice, the calculations are time-consuming, are complex beyond easy comprehension, and generally do not give accurate representation of the thermodynamic functions. The failure of the method for most substances of geologic interest arises mainly from our lack of adequately detailed knowledge of atomic interactions and from the inherent complexity of minerals, which are polyatomic and of low symmetry.

In this series of papers a new approach is proposed to the problem of relating data on elastic constants, spectroscopic properties, thermodynamic functions, and phase equilibria. This approach has its roots in lattice dynamics theory but lacks its rigor and elegance. In exchange, it offers relative simplicity, utility, and, it is hoped, comprehensibility for problems of mineral thermodynamics.

The thermodynamic functions of a crystal (e.g., Helmholtz free energy $F$, internal energy $E$, heat capacity $C_V$, and entropy $S$) can, in the harmonic approximation, be expressed as averages over the frequency spectrum $g(\omega)$; these functions are given by the expressions shown in Table 1. The motivating

---

TABLE 1.    Harmonic Expressions for the Thermodynamic Functions

| Thermodynamic Function | Relation to the Partition Function $Z$ for a System of Independent Oscillators | Expression in Terms of Exponential Functions | Expression in Terms of Hyperbolic Functions |
|---|---|---|---|
| $E$ (internal energy) | $E = kT^2 \dfrac{\partial \ln Z}{\partial T}$ | $E = -3nN_A\beta + \displaystyle\int_0^{\omega_L} \dfrac{\hbar\omega}{e^{\hbar\omega/kT} - 1} g(\omega)\, d\omega$ | $E = -3nN_A\beta + \dfrac{\hbar}{2}\displaystyle\int_0^{\omega_L} \omega \coth \dfrac{\hbar\omega}{2kT} g(\omega)\, \dfrac{d\omega}{2\pi}$ |
| $C_V$ (heat capacity) | $C_V = \dfrac{k}{T^2} \dfrac{\partial^2 \ln Z}{\partial(1/T)^2}$ | $C_V = k \displaystyle\int_0^{\omega_L} \dfrac{e^{\hbar\omega/kT}}{(e^{\hbar\omega/kT} - 1)^2}\left(\dfrac{\hbar\omega}{kT}\right)^2 g(\omega)\, d\omega$ | $C_V = k \displaystyle\int_0^{\omega_L}\left(\dfrac{\hbar\omega}{2kT}\right)^2 \mathrm{csch}^2 \dfrac{\hbar\omega}{2kT} g(\omega)\, \dfrac{d\omega}{2\pi}$ |
| $S$ (entropy) | $S = \dfrac{E}{T} + k \ln Z$ | $S = \dfrac{1}{T}\displaystyle\int_0^{\omega_L} \dfrac{\hbar\omega}{e^{\hbar\omega/kT} - 1} g(\omega)\, d\omega$ $- k \displaystyle\int_0^{\omega_L} \ln(1 - e^{-\hbar\omega/kT}) g(\omega)\, d\omega$ | $S = k \displaystyle\int_0^{\omega_L}\left\{\dfrac{\hbar\omega}{2kT} \coth \dfrac{\hbar\omega}{2kT}\right.$ $\left. - \ln\left[2 \sinh \dfrac{\hbar\omega}{2kT}\right]\right\} g(\omega)\, \dfrac{d\omega}{2\pi}$ |
| $F$ (Helmholtz free energy) | $F = -kT \ln Z$ | $F = 3nN_A\beta + kT\displaystyle\int_0^{\omega_L} \ln(1 - e^{-\hbar\omega/kT}) g(\omega)\, d\omega$ | $F = 3nN_A\beta + kT\displaystyle\int_0^{\omega_L} \ln\left\{2 \sinh \dfrac{\hbar\omega}{2kT}\right\} g(\omega)\, \dfrac{d\omega}{2\pi}$ |

The expressions in terms of exponential functions are after *Reif* [1965, chapter 10], and those in terms of hyperbolic functions are after *Maradudin et al.* [1963, p. 46]. The partition function $Z$ is given by $\ln Z = 3kTnN_A\beta - \int_0^{\omega_L} \ln(1 - e^{-\hbar\omega/kT})g(\omega)\, d\omega$. In the expression for $E$ in terms of exponential functions, $-3nN_A\beta = V_0 + \frac{1}{2}\sum_{r=1}^{3N_A n} \hbar\omega_e$, where $V_0$ is the potential energy of the equilibrium configuration of oscillators; the summation term is the zero-point energy. In the equations of the table, $n$ is the number of atoms in the chemical formula; $N_A$ is Avogadro's number; $\hbar$ is the Planck constant $h$ divided by $2\pi$; $k$ is the Boltzmann constant; $T$ is the temperature in degrees Kelvin; $\omega$ is the frequency; $\omega_L$ is the maximum lattice vibrational frequency; and $g(\omega)\, d\omega$ is the fraction of frequencies in the interval $(\omega, \omega + d\omega)$. Note that the normalization to $3N_A n$ degrees of freedom is contained in the expression for $g(\omega)$ rather than in the partition function except for the zero-point energy term.

force for proceeding with a less rigorous model than the complete lattice dynamics formulation for lattice vibrations of minerals is the well-known fact that because the thermodynamic functions are averages over the frequency spectrum, they are insensitive to details of the spectrum.

The Debye model of the lattice vibrational spectrum, which gives a $g(\omega)$ that is a quadratic function of frequency, has been used commonly in geologic studies to predict or extrapolate the heat capacity or entropy of minerals and to relate their thermal properties to acoustic velocities. In this series of papers it is demonstrated that for most minerals a Debye model is inadequate to specify thermal properties which depend on lattice vibrations. The spectrum proposed as an alternative to the Debye spectrum is somewhat more complicated but is, nevertheless, still reasonably convenient. It is able to account much better than the Debye model for the variation of the thermodynamic properties of complex substances over a wide range of temperatures. In this paper, Debye theory is reviewed to provide a basis for the model introduced, measured heat capacities of simple and complex substances are compared, causes of deviations from Debye behavior are investigated, and simple quantitative models for one-dimensional lattices are discussed to provide a basis for the model introduced in paper 3 [*Kieffer*, 1979c].

## 2.   TEMPERATURE DEPENDENCE OF THE HEAT CAPACITY OF COMPLEX SUBSTANCES

### Debye Model

Of the many analytic models proposed for frequency distributions of lattice vibrations, one of the most enduring, because of its simplicity and universal applicability to simple substances, was developed by *Debye* [1912]. Debye developed the theory of distribution of frequencies in a solid by considering the solid as an isotropic elastic continuum. At the time of Debye's original paper on this subject the theory of reciprocal

lattices and zones was not known, although Born had obtained some of the main results in a simultaneous alternative formulation of a specific heat theory [*Born and von Karman*, 1912, 1913]. The derivation presented below gives recognition to the underlying crystal lattice, as treated in the lattice dynamical theory of *Born and von Karman* [1912], and thus emphasizes the approximations made to actual lattice structure [*Brillouin*, 1953]. For further details, see the work of *Maradudin et al.* [1963].

Consider a primitive Bravais lattice with basis vectors $a_1$, $a_2$, $a_3$ forming the edges of the cells (symbols are defined in the notation list). A corresponding reciprocal lattice is defined by the reciprocal basis vectors

$$b^1 = \frac{2\pi a_2 \times a_3}{|a_1 \cdot a_2 \times a_3|},$$

$$b^2 = \frac{2\pi a_3 \times a_1}{|a_2 \cdot a_3 \times a_1|} \qquad (1)$$

$$b^3 = \frac{2\pi a_1 \times a_2}{|a_3 \cdot a_1 \times a_2|}$$

(In crystallographic literature the factor $2\pi$ is omitted from the above expressions. However, it is convenient to include this factor in treatments of the interaction of waves with periodic lattices, as will be seen in section 3.)

The wave vectors for lattice vibrational waves are conveniently represented in reciprocal space in the form [e.g., *Kittel*, 1968, p. 53]

$$K(\eta) = \eta_1 b^1 + \eta_2 b^2 + \eta_3 b^3 \qquad (2)$$

(where the $\eta_i$ are integers and $K$ is a reciprocal lattice vector). The unit cell of the direct lattice, with volume $V_L$, may be represented in the reciprocal lattice by a unit cell whose volume $V_R$ is inversely proportional to the volume of a unit cell of

the direct lattice, $V_R = (2\pi)^3/V_L$. The reciprocal unit cell is called the Brillouin zone. Its boundaries are usually chosen symmetrically about the origin of the reciprocal lattice, $\mathbf{K} = 0$. The Brillouin zone is identical to the usual reciprocal cell adopted by crystallographers except that the factor of $2\pi$ is included, the origin is taken at the center of the cell rather than at a corner, and the wave vector $\mathbf{K}$ is a coordinate rather than a reciprocal length.

Let us now consider the propagation of elastic waves through a lattice. It is well known [e.g., *Brillouin*, 1953] that all elastic vibrations of a lattice propagate as waves of the form

$$\mathbf{u}(\mathbf{x}, t) = A\hat{n} \sin (\mathbf{K}\cdot\mathbf{x} - \omega t + \delta)$$

where $\mathbf{u}(\mathbf{x}, t)$ is the displacement of the medium at the point $\mathbf{x}$ and time $t$, $\omega$ is the frequency, $\hat{n}$ is the direction in which the displacements occur, $\mathbf{K}$ is the wave vector, $A$ is an amplitude, and $\delta$ is a phase factor. In general, the frequency $\omega$ of lattice vibrations is a function of the direction and magnitude of the wave vector $\mathbf{K}$. The wave velocity (the group velocity) $v$ is given by

$$|v| = \partial\omega/\partial|\mathbf{K}| \tag{3}$$

The relation between $\omega$ and $\mathbf{K}$ (or $\nu = \omega/2\pi$ and $\mathbf{y} = \mathbf{K}/2\pi$) is called the dispersion relation. The Debye theory assumes that all modes of vibration are acoustic and all have the same wave velocity $v$ (Figure 1a). These waves are dispersionless; i.e., phase velocities and group velocites are the same.

The Debye theory also assumes that the vibrational states of the crystal correspond to wave vectors $\mathbf{K}$ whose tips are uniformly distributed in reciprocal space. Because the available volume in reciprocal space increases proportionally to $|\mathbf{K}^2|d\mathbf{K}$, the density of vibrational states, $f(\mathbf{K})$, has the form

$$f(\mathbf{K})\, d\mathbf{K} = 4\pi\mathbf{K}^2\, d\mathbf{K}\cdot d$$

where $d$ is the density (assumed uniform) of wave vectors in reciprocal space. The density of states $g(\omega)$, expressed in terms of the vibrational frequency $\omega = v\mathbf{K}$, can therefore be written

$$g(\omega)\, d\omega = f[\mathbf{K}(\omega)]\, \frac{d\mathbf{K}}{d\omega}\, d\omega = a\omega^2\, d\omega \tag{4}$$

where $a$ is a constant that depends on the elastic wave velocities. Here $g(\omega)\, d\omega$ is the number of vibrational states lying between $\omega$ and $\omega + d\omega$. The parabolic form of $g(\omega)$ is illustrated in Figure 1b. The simple parabolic form of the vibrational spectrum in (4) is the central feature of the Debye model, and it is valid for any crystal in the limit as $\omega \to 0$ (long-wavelength phonons).

The value of $a$ in (4) is determined by the density of vibrational states in reciprocal space. All normal modes of the
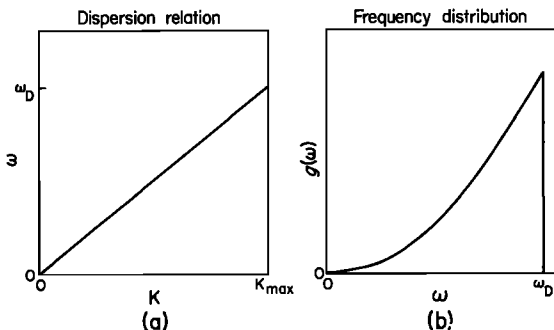


Fig. 1. (a) Schematic dispersion relation for Debye solid (arbitrary units). (b) Schematic spectral density $g(\omega)$ for a Debye solid.

crystal are represented by wave vectors within one reciprocal cell because only those vibrational modes are physically distinct. A crystal consisting of one mole of the substance of interest contains $nN_A$ atoms, where $n$ is the number of atoms in the chemical formula and $N_A$ is Avogadro's number, and it has $3nN_A$ normal modes of vibration. As was just stated, the wave vectors corresponding to these normal modes span one reciprocal cell. The molar density $d$ of vibrational states in reciprocal space is thus

$$d = 3nN_A/V_R = 3nN_A V_L/(2\pi)^3 = 3nZV/(2\pi)^3$$

where $V$ is the molar volume of the crystal and $Z$ is the number of formula units in the unit cell ($V_L = VZ/N_A$). When it is transformed to the frequency representation by (4), this density corresponds to a value of $a$ given by

$$a = 3nZV/2\pi^2 v_M{}^3 \tag{5}$$

As was previously stated, this assumes that all acoustic waves have the same speed $v_M$ and hence that the crystal is elastically isotropic. In reality, the compressional ($P$) and shear ($S$) waves have separate speeds, so that for an isotropic crystal there are two separate spectral contributions of the type (4), one with $a_p = nZV/2\pi^2 v_p{}^3$ and the other with $a_S = 2nZV/2\pi^2 v_S{}^3$. For simplicity, in Debye theory this more complicated spectrum is often replaced by a single spectrum with an averaged value of $a$:

$$a = \frac{3nZV}{2\pi^2 v_M{}^3} = \frac{nZV}{2\pi^2}\left(\frac{1}{v_P{}^3} + \frac{2}{v_S{}^3}\right) \tag{6}$$

Most crystals are elastically anisotropic, so that for each wave propagation direction $\mathbf{K}$ there are three, rather than two, distinct wave velocities, $v_1(\mathbf{K})$, $v_2(\mathbf{K})$, and $v_3(\mathbf{K})$. In a simple Debye' theory the separate spectral contributions from these different waves are averaged by using a mean velocity

$$\frac{3}{v_M{}^3} = \frac{1}{4\pi}\int\left(\frac{1}{v_1{}^3} + \frac{1}{v_2{}^3} + \frac{1}{v_3{}^3}\right)d\Omega \tag{7}$$

where the integration is over all directions of $\mathbf{K}$, $d\Omega$ being an increment of solid angle about the origin of the Brillouin zone. To accomplish in a simple way the averaging represented by (7), it has become common practice in geophysics to use the Voigt-Reuss-Hill (VRH) average velocity for $v_M$ in (7) [see O. L. Anderson, 1963].

In the Debye model, the Brillouin zone is simplified by replacing the actual zone with a sphere of the same volume in reciprocal space, centered at the origin of the reciprocal lattice. Its radius $K_{max} = |\mathbf{K}_{max}|$ is thus given by

$$\tfrac{4}{3}\pi K_{max}{}^3 = (2\pi)^3/V_L \tag{8}$$

Corresponding to the maximum wave vector $K_{max}$ is a maximum frequency $\omega_D$ given by the dispersion relation $\omega_D = v_M K_{max}$. In the simplest form, using (5), a sharp cutoff frequency $\omega_D$ is given by

$$\omega_D = v_M K_{max} = v_M\left(6\pi^2\,\frac{N_A}{ZV}\right)^{1/3} = \left(\frac{9nN_A}{a}\right)^{1/3} v_M \tag{9}$$

($N$ is the number of atoms in one mole of the crystal; $N = nN_A$.) This cutoff frequency is the quantity normally used to characterize the Debye spectrum of a crystal, and it is usually given in terms of the Debye temperature $\theta_D$, defined as follows:

$$\theta_D = \hbar\omega_D/k \tag{10}$$

where $\hbar$ is Planck's constant $h$ divided by $2\pi$ and $k$ is the

Boltzmann constant. The Debye temperature calculated from (9) and (10) on the basis of acoustic velocities is called the elastic Debye temperature to distinguish it from Debye temperatures estimated on the basis of specific heat data or by other means. From (5), (9), and (10) it follows that the Debye temperature can be calculated from

$$\theta_D = \frac{\hbar}{k}\left(\frac{6\pi^2 N_A}{ZV}\right)^{1/3} v_M \tag{11}$$

The specific heat of a solid is obtained by considering the heat capacity contribution $C_V{}^E$ of the individual lattice vibrational oscillators ('Einstein oscillators') of frequency $\omega$:

$$C_V{}^E = \frac{\partial}{\partial T}\left[\frac{\hbar\omega}{\exp(\hbar\omega/kT)-1}\right] \equiv \varepsilon\left(\frac{\hbar\omega}{kT}\right) \tag{12a}$$

where

$$\varepsilon\left(\frac{\hbar\omega}{kT}\right) = \frac{(\hbar\omega/kT)^2 \exp(\hbar\omega/kT)}{[\exp(\hbar\omega/kT)-1]^2} \tag{12b}$$

$\varepsilon(\hbar\omega/kT)$ is defined as the Einstein (heat capacity) function and $T$ is the absolute temperature. The molar heat capacity is a summation of Einstein functions for all of the oscillators:

$$C_V = \int_0^{\omega_D} g(\omega)\,\varepsilon\left(\frac{\hbar\omega}{kT}\right) d\omega \tag{13}$$

For a Debye solid, with $g(\omega)$ given by (4) and (5), the specific heat in (13) can be written with the use of (9) in the dimensionless form as

$$C_V = 9nN_A k \frac{T^3}{\theta_D{}^3}\int_0^{\theta_D/T} \frac{e^x}{(e^x-1)^2} x^4\,dx = 3nN_A k D(\theta_D/T) \tag{14}$$

where $x = \hbar\omega/kT$. The function $D(\theta_D/T)$ defined by this equation, frequently called the Debye (heat capacity) function, is tabulated in many references [e.g., Gopal, 1966]. From the Debye function and a knowledge of the acoustic velocities (which gives the Debye temperature $\theta_D$) the heat capacity as a function of temperature can be predicted if the vibrational frequencies of the solid follow a parabolic frequency distribution.

The low-temperature and high-temperature limits of the thermodynamic functions are of particular interest in geology and geophysics, the low-temperature limit because it strongly influences the entropy and the high-temperature limit because it applies to most subcrustal conditions. At temperatures well below the Debye temperature ($T \ll \theta_D$ so that $\hbar\omega_D/kT \gg 1$) the upper limit in the integral $D(\theta_D/T)$ can be replaced by infinity. The resulting integral is simply a constant (evaluated in several ways by Reif [1965, Appendix A11]). At low temperatures the heat capacity has the well-known form

$$C_V = \frac{12\pi^4}{5}nN_A k \frac{T^3}{\theta_D} \tag{15}$$

This equation is referred to as the 'Debye $T^3$ law.' At high temperatures, $D(\theta_D/T)$ approaches 1, and the molar heat capacity approaches a constant value $3nR$, the Dulong-Petit limit. ($R$ is the gas constant, 1.9877 cal mol$^{-1}$ deg$^{-1}$.) The low- and high-temperature limits of the thermodynamic functions for a Debye solid are given in Table 2.

The Debye model can be tested by comparing any of the thermodynamic functions calculated from Table 2 with measured values. This comparison is usually made by comparing the predicted heat capacity with the measured heat capacity data as described in the next section.

### Applicability of the Debye Model

Applicability of the Debye model to real substances is governed by the extent to which the actual lattice vibrational spectrum is approximated by the $g(\omega)$ given by (4) and (5), with the assumed sharp upper cutoff frequency $\omega_D$ given by (9). Mathematical models of the vibrational modes of crystalline arrays of atoms [Blackman, 1955] show that for monatomic substances, in which there is only one atom per unit cell (which allows the choice $n = 1$ and $Z = 1$ in (5), (6), (9), (11), (14), and (15)), the vibrational spectrum is reasonably well represented by the Debye model. The separate spectral contributions from the $P$ and $S$ vibrations cause a definite departure from the simple Debye spectrum at the higher frequencies; however, the form of the dispersion relation for the individual branches ($P$ or $S$) departs from the linearity assumed in the Debye model in such a way as to tend to compensate the effect of the separate $P$ and $S$ waves [see Leibfried, 1955, p. 251].

A similar conclusion follows for polyatomic solids ($n > 1$) if the different atoms play nearly equivalent mechanical roles in the vibrational process. In general terms, the conditions for mechanical equivalence are that (1) the various atoms have nearly equal masses, (2) the coordination environments of the different atoms are nearly identical, (3) the environments are essentially isotropic, and (4) the various near-neighbor interatomic force constants are nearly equal. If these conditions hold, it is possible to think of the polyatomic crystal as essentially a monatomic crystal as far as the atomic vibrations are concerned; the 'vibrational unit' of the crystal can be taken as the individual atom without regard to type.

For more complex substances the failure of one or more of conditions 1–4 above results in such large changes in the vibrational spectrum that the Debye model no longer provides an adequate approximation to the vibrational spectrum or to the heat capacity. The extent of departure from Debyelike behavior is shown by the widely used procedure of representing the observed $C_V$ at each temperature in terms of a so-called 'calorimetric Debye temperature' $\theta_{cal}(T)$, which is the value of

TABLE 2. Harmonic Expressions for the Thermodynamic Functions of a Debye Solid

| Function | Low-Temperature Limit | High-Temperature Limit |
|---|---|---|
| $E = -3nN_A\beta + 3nN_A kT D(\theta_D/T)$ | $E = -3nN_A\beta + (3\pi^4/5)nN_A k(T^4/\theta_D{}^3)$ | $E = -3nN_A\beta + 3nN_A kT$ |
| $C_V = 3nN_A k D(\theta_D/T)$ | $C_V = (12\pi^4/5)nN_A k(T/\theta_D)^3$ | $C_V = 3nN_A k$ |
| $S = -3nN_A k \ln(1 - e^{-\theta_D/T}) + 4nN_A k D(\theta_D/T)$ | $S = (4\pi^4/5)nN_A k(T/\theta_D)^3$ | $S = -3nN_A k \ln(\theta_D/T) + 4nN_A k$ |
| $F = -3nN_A\beta + 3nN_A kT \ln(1 - e^{-\theta_D/T}) - 3nN_A kT D(\theta_D/T)$ | $F = -3nN_A\beta - (3\pi^4/5)nN_A k(T^4/\theta_D{}^3)$ | $F = -3nN_A\beta + 3nN_A kT \ln(\theta_D/T) - nN_A kT$ |

For a Debye solid the partition function $Z$ is given by $\ln Z = 3kTnN_A\beta - 3nN_A \ln(1 - e^{-\theta_D/T}) + 3nN_A(T^3/\theta_D{}^3)\int_0^{\theta_D/T}(x^3\,dX)/(e^x - 1) = 3kTnN_A\beta - 3nN_A \ln(1 - e^{-\theta_D/T}) + nN_A D(\theta_D/T)$. This equation contains the definition of $D(\theta_D/T)$, which is the derivative of the Debye function $D(\theta_D/T)$ [Reif, 1965]. $D(\theta_D/T) = (3T^3/\theta_D{}^3)\int_0^{\theta_D/T}(x^3\,dx)/(e^x - 1)$ and $D(\theta_D/T) = 3(T^3/\theta_D{}^3)\int_0^{\theta_D/T}(x^4 e^x dx)/(e^x - 1)^2$.
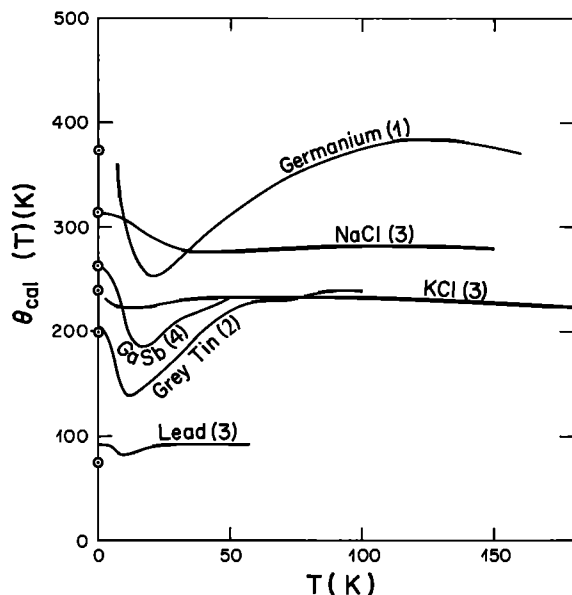
Fig. 2. Calorimetric Debye temperature $\theta_{cal}(T)$ for simple, nearly Debyelike substances. Elastic Debye temperatures $\theta_{el}$ for 0°K are shown by circles. Values of $\theta_{cal}(T)$ were calculated from $C_V$ from the following references: curves 1 and 2, Ge and Sn [Hill and Parkinson, 1952]; curves 3, NaCl, Pb, and KCl [Blackman, 1955]; and curve 4, GaSb [Cetas et al., 1968].

$\theta_D$ in (14) that will reproduce the observed $C_V(T)$. Katz [1951] has shown that in the low-temperature range $0 < T < \theta/10$, peaks and dips in the $\theta_{cal}(T)$ curves represent dips and peaks, respectively, in the low-frequency part of the vibrational spectrum. The $\theta_{cal}(T)$ curves are especially useful in showing differences between models and data at very low temperatures where the magnitude of $C_V$ is small. However, at high temperatures where $C_V$ approaches the Dulong-Petit limit, the $\theta_{cal}(T)$ curves overemphasize small differences between models. For example, at $T \sim \theta_D$ a 1% difference in $C_V$ gives a difference of nearly 10% in $\theta_{cal}(T)$ [Gopal, 1966, p. 195]. Examples of $\theta_{cal}(T)$ for simple, rather Debyelike solids and for solids of geological interest are shown in Figures 2 and 3.

### Elastic Debye Temperature

A stringent test of the Debye model lies in its quantitative prediction of the heat capacity in terms of the elastic properties: $\theta_{cal}$ should be the same as $\theta_D$ calculated from the sound velocities via (11). To make the distinction explicit, Debye temperatures calculated in this way from elastic data (or the corresponding sound velocities) are often called 'elastic Debye temperatures' and are here designated with the symbol $\theta_{el}$. Because the elastic constants vary somewhat with temperature, a temperature dependence should be considered for $\theta_{el}(T)$, but the dependence is usually slight enough to be ignored for most purposes [O. L. Anderson, 1963]. In calculating $\theta_{el}$ from (11) for simple compounds satisfying conditions 1-4 stated above, it is the practice to take $nN_A/V$ as the particle density (number of atoms per unit volume without regard to type), in accordance with the rationale discussed, in which the 'vibrational unit' of the crystal is the single atom without regard to type. This practice has generally been followed also in calculating $\theta_{el}$ for minerals, as in the examples cited above, even though conditions 1-4 generally do not hold for these substances.

In principle, $\theta_{cal}(0) = \theta_{el}$ for an anisotropic solid when the appropriate mean sound velocity is used (equation (7)) [Born and Huang, 1954, p. 62]. No assumption of waves propagating

with a velocity that is an average of $v_P$ and $v_S$ is needed because at sufficiently low frequencies the separate contributions of the $P$ and $S$ waves to $g(\omega)$ simply add in accordance with (7). A 'Debyelike' $T^3$ region is predicted even for highly anisotropic substances at sufficiently low temperatures.

Any elastic anisotropy requires a detailed summation of the contributions to $g(\omega)$ for waves traveling in different directions. There is no reason to expect that this summation would lead exactly to the same result as is obtained by the common practice of substituting into (7) or (11) values of $v_P$ and $v_S$ obtained by taking Voigt-Reuss-Hill averages for elastically anisotropic crystals or by taking $v_P$ and $v_S$ measured on polycrystalline samples. In a few cases (e.g., rutile and calcite [Robie and Edwards, 1966]) where $v_M$ has been calculated it is found to be close to the Voigt-Reuss-Hill average and between the Voigt and Reuss limits. Thomsen [1972] has reviewed the problem of the equivalence of single-crystal and polycrystalline data. In general, there are insufficient data to permit the required integrations in (7) to be performed for solids of geological interest, and the use of the VRH velocities is required. Because all crystals are elastically anisotropic to some degree, some discrepancy (although perhaps slight) may be expected between $\theta_{cal}(0)$ and $\theta_{el}$ as conventionally calculated from the average in (6) or as calculated from VRH or polycrystalline data.

At low frequencies the shear branches contribute more significantly to the specific heat than the longitudinal branch. O. L. Anderson and R. C. Liebermann [1966] have discussed the relative importance of $v_S$ and $v_P$ in the determination of $\theta_{el}$ and conclude that for materials of normal Poisson's ratio $\sigma_P$ (0.15 $< \sigma_P < 0.35$), $\theta_{el}$ can be adequately approximated from a knowledge of $v_S$ and an assumed $\sigma_P$, because the dependence of $\theta_{el}$ on $v_P$ through $\sigma_P$ is slight.

The $\theta_{el}$ values marked in Figure 3 by the circles have been obtained for the most part from elastic or acoustic measurements at room temperature, but, as was noted above, they can



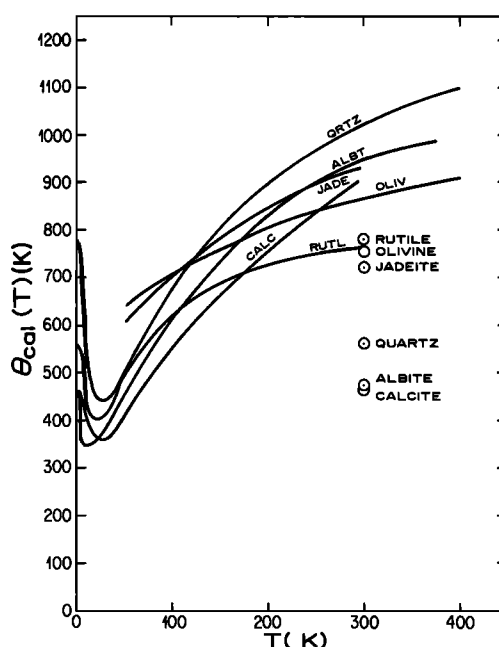Fig. 3. Values of $\theta_{cal}(T)$ for representative minerals. Note the change in ordinate scale from Figure 2. Additional data are shown in Figure 4. Room temperature elastic values $\theta_{el}$ are shown by circles at 300°K; they are assumed to apply at low temperatures as well. References to specific heat data from which the $\theta_{cal}(T)$ curves were calculated are given in the caption to Figure 4.

be considered appropriate over a wide temperature range, because the temperature variation of particle density and sound velocity is slight. For elements and simple compounds that are Debyelike in showing a nearly temperature-independent $\theta_{cal}(T)$ it is found that $\theta_{el}$ generally agrees with $\theta_{cal}$ to within 10% [Blackman, 1955]. Alers [1965] has shown that $\theta_{el}$ and $\theta_{cal}$ should be in reasonable agreement ($|(\theta_{el} - \theta_{cal})/\theta_{el}|$ < $0.02\theta_{el}$) for $T < \theta_D/50$ in the case of the cubic metals, for $T < \theta_D/100$ in the case of alkali halides, and for $T < \theta_D/150$ in the case of the hexagonal metals. The 2% latitude quoted by Alers [1965] in the agreement between $\theta_{el}$ and $\theta_{cal}$ may arise from difficulties in obtaining accurate elastic constants, in extrapolating them to $0°K$, and in measuring the heat capacity accurately to the very low temperatures required to obtain a reliable value of $\theta_{cal}(0)$.

For minerals, data are relatively sparse, but a similar agreement between $\theta_{cal}(0)$ and $\theta_{el}$ is found. Very low temperature heat capacity data and elastic constants are available for quartz, silica glass, calcite, rutile, albite, microcline, muscovite, coesite, and stishovite. In all cases, $\theta_{cal}(0)$ appears to approach $\theta_{el}$ within 10%. Hence the equality of $\theta_{cal}(0)$ and $\theta_{el}$ appears to hold for silicates.

### Constancy of the Debye Temperature

For those elements and alkali halides to which the Debye model may be expected to apply, $\theta_{cal}(T)$ should be a constant equal to $\theta_D$. The near constancy of $\theta_{cal}(T)$ for Pb, KCl, and NaCl in Figure 2, particularly at the higher temperatures, is about as close an approach to ideal Debye behavior as is achieved for any real solids. The $\theta_{cal}(T)$ curves for Ge, gray Sn, and GaSb are examples of about the largest departures from ideal Debye behavior that are found for elements or simple compounds, excluding molecular solids such as $I_2$. Most simple compounds show significant departures from ideal Debye behavior over a range of temperatures just above $0°K$. In this range, $\theta_{cal}(T)$ typically drops by a few percent to, at most, 25% from its value at absolute zero [Donovan and Angress, 1971]. The curve for Ge in Figure 2 shows a relatively exaggerated example of this type of behavior for a simple solid. For most simple solids, $\theta_{cal}(T)$ becomes essentially constant at the value $\theta_{el}$ for $T > 0.1\theta_D$. A detailed discussion of these points is given by Blackman [1955].

The general agreement of the $\theta_{cal}(T)$ curves of the simple substances with the predictions of the Debye model (i.e., the $0°K$ value and the constancy of $\theta_{cal}(T)$) suggests that the parabolic representation of the vibrational spectrum is adequate for prediction of the thermodynamic properties for these substances which satisfy the four criteria listed earlier. In those cases where complete vibrational spectra of simple substances have been obtained (either by detailed theoretical models or by integration of inelastic neutron scattering data) the overall agreement with the Debye spectrum is good. Examples of spectra for halite and periclase are given in paper 2 [Kieffer, 1979b].

Minerals in general show a very different behavior: a few examples are shown in Figure 3. The $\theta_{cal}(T)$ curves show a pronounced minimum at temperatures of a few degrees Kelvin and, with increasing temperature, an asymptotic approach toward a value greatly exceeding $\theta_{cal}(0)$ or $\theta_{el}$. Typically, $\theta_{cal}(T)$ drops by 20-50% from its value at absolute zero before rising toward the high-temperature limit. The asymptotic limit is usually approached at temperatures greater than $\theta_{cal}(0)/2$, i.e., at temperatures much higher than those at which the 'simple' substances begin to show a constant $\theta_{cal}(T)$. The

calorimetric behavior of the minerals may be examined somewhat more systematically by plotting $\theta_{cal}(T)$, normalized to $\theta_{el}$, as a function of temperature $T$. Such curves for most of the minerals studied in this work are shown in Figure 4. They were calculated from $C_P$ data referenced in the figure caption. The method of correction of $C_P$ to $C_V$ (required for calculation of $\theta_{cal}(T)$) is given in paper 3.

Consider first in Figure 4 the final high-temperature limit attained ($\theta_{cal}(\infty)$) and the rate at which the curves rise toward this limit. This can be done by considering, for example, the temperature at which $\theta_{cal}(T)/\theta_{el}$ regains the value unity or by considering the relative slopes of the curves as they rise. Both the high-temperature limit and the rate of rise toward this limit are greatest for framework silicates, less for chain and orthosilicates, and least for the aluminum oxides, corundum and spinel. The high-temperature limit is generally $1100°-1200°K$ for the framework silicates, between $\sim1000°$ and $1100°$ for the chain and orthosilicates, and about $950°$ for spinel and corundum. Enstatite, zircon, and sillimanite are notable exceptions, discussed below.

Generalizations about calorimetric trends at low temperatures in Figure 4 are much more tentative because of the scarcity of low-temperature calorimetric data. In general, as the temperature decreases from high values, the $\theta_{cal}(T)/\theta_{el}$ curves drop below unity, and the curves must therefore show a minimum at low temperatures, because they must regain the value of unity at $0°K$. Two systematics appear.

1. The depth of the minimum attained appears to be greatest for the framework silicates (the value of $\theta_{cal}(T)/\theta_{el}$ at the minimum is 0.71 for quartz, 0.67 for coesite, 0.71 for cristobalite, 0.74 for albite, and 0.76 for microcline), is probably smaller for the chain and sheet silicates (about 0.80-0.82 for muscovite, jadeite, and diopside), and least for the orthosilicates (inferred to be about 0.80 for olivine and sillimanite and 0.90 for zircon, kyanite, and andalusite). The dip is relatively small for the oxides (0.90 for periclase, 0.87 for corundum, and 0.89 for spinel) and is comparable to the small values observed for simple substances (0.95 for halite). Stishovite shows a very large dip, but the data are suspect at very low temperatures because of the extremely small particle size (740 Å) used in the heat capacity experiments [Holm et al., 1967]. Rutile also shows a very large dip in the $\theta_{cal}(T)/\theta_{el}$ curve, apparently due to an anomalously temperature-dependent optical mode, one of many anomalies observed and attributed to the high polarizability of the titanium ion [Traylor et al., 1971]. Silica glass has long been known to have an excess heat capacity relative to that of crystalline quartz (discussed in paper 3), and this is apparent in the large dip in its $\theta_{cal}(T)$ curve. An extraordinary exception to the trends noted above for the silicates is pyrope, for which $\theta_{cal}(T)/\theta_{el}$ drops to 0.34. This anomaly, which gives rise to a high entropy for pyrope compared to that expected by entropy-estimating schemes, may be associated with anomalous vibrations of loosely bound magnesium atoms in the pyrope structure [Kieffer, 1979a].

2. The second systematic trend is that the temperature at which the minimum is attained is generally lowest for framework silicates ($T_{min} = 20°$ for quartz and coesite; $T_{min} \sim 15°$ for cristobalite, albite, and microcline), higher for sheet and chain silicates ($\sim30°$ for muscovite, perhaps $20°-40°$ for jadeite and diopside), and highest for orthosilicates (perhaps $20°-40°$ for olivine and zircon, $\sim55°$ for kyanite, and $\sim40°-50°$ for andalusite and sillimanite). Broad minima for the oxides corundum and spinel occur at $60°-70°K$, and even broader minima occur for halite and periclase at $80°-100°$ and $100°$,
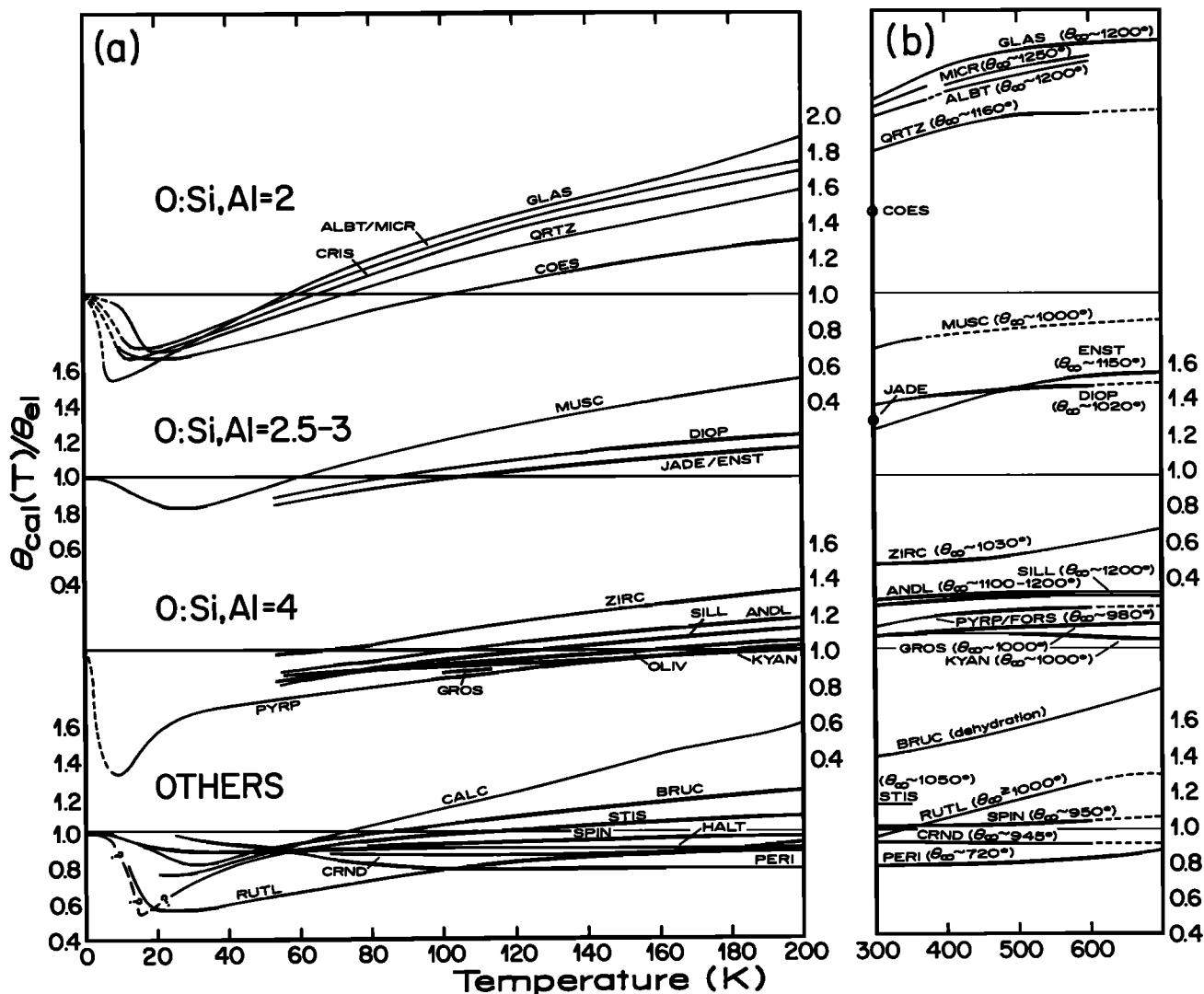
Fig. 4. Curves of $\theta_{cal}(T)/\theta_{el}$ versus $T$ for (a) low-temperature data, and (b) high-temperature data (abscissa scale different from that in Figure 4a). Extrapolated curves are dashed. $C_P$ data from the sources listed below were corrected to $C_V$ through $C_V = C_P - TV\alpha^2B$, where $T$, $V$, $\alpha$, and $B$ are the temperature, volume, thermal expansion, and bulk modulus, respectively. Where data were available, $\alpha$ and $B$ were represented as $\alpha = \alpha_1 + \alpha_2T^2$ and $B = B_0 + dB/dT$. High-temperature values for halite are not shown because of uncertainties introduced into the correction from $C_P$ to $C_V$ by lack of thermodynamic data (see paper 3 for discussion). High-temperature values for coesite and stishovite are not available because of metastability of these phases. High-temperature enstatite data may be influenced by an ortho-clino transition. The andalusite high-temperature data are uncertain because the thermal expansion is not known. The curves for albite and microcline and for jadeite and enstatite are indistinguishable at low temperature. The pyrope trend is believed to be anomalous for an orthosilicate for reasons discussed in paper 4 (S. W. Kieffer, manuscript in preparation, 1979). The values of $\theta_\infty$ shown were obtained by linearly extrapolating the value at 600° or 700°K to 1000°K with a gradient equal to that at 500°-700°K. This procedure was adopted because, in general, even when $C_P$ data are available to 1000°K, the correction from $C_P$ to $C_V$ is too uncertain to give reliable estimates of $\theta_{cal}(\infty)$. (Remember that at these temperatures a 1% variation in $C_V$ can give a 10% variation, or ~100° variation, in $\theta_{cal}(T)$.) Sources of data used are halite (HALT) [Clusius et al., 1949]; periclase (PERI) [Barron et al., 1959]; brucite (BRUC) [Giauque and Archibald, 1937]; corundum (CRND) [Ginnings and Furukawa, 1953]; quartz (QRTZ) [Lord and Morrow, 1957, quoting unpublished data of E. F. Westrum]; cristobalite (CRIS) [C. T. Anderson, 1936]; silica glass (GLAS) [Lord and Morrow, 1957, quoting unpublished data of E. F. Westrum; Flubacher et al., 1959]; coesite (COES) [Holm et al., 1967]; stishovite (STIS) [Holm et al., 1967]; rutile (RUTL) [Sandin and Keesom, 1969; Pandey, 1965; Dugdale et al., 1954; Shomate, 1947; Keesom and Pearlman, 1958]; albite (ALBT) [Openshaw, 1974; Kelley et al., 1953]; microcline (MICR) [Openshaw, 1974; Kelley, 1960]; spinel (SPIN) [King, 1955; Bonnickson, 1955]; jadeite (JADE) [Kelley et al., 1953]; diopside (DIOP) [King, 1957]; enstatite (ENST) [Kelley, 1943]; olivine (OLIV) [Kelley, 1943; Orr, 1953]; zircon (ZIRC) [Kelley, 1941]; kyanite (KYAN), andalusite (ANDL), and sillimanite (SILL) [Simon and Zeidler, 1926] (later data by Todd [1950] give somewhat higher curves); pyrope (PYRP), grossular (GROS), and andradite (ANDR) [Kiseleva et al., 1972]; and calcite (CALC) [C. T. Anderson, 1934; Stavely and Linford, 1969].

respectively. For pyrope the position of its minimum, as well as its depth, is anomalous in comparison to that of the other orthosilicates.

These departures from behavior expected from the Debye model imply deviations of the vibrational spectrum from the parabolic spectrum assumed by Debye. As was noted earlier,

the dip in the $\theta_{cal}(T)/\theta_{el}$ curve at low temperature corresponds to excess oscillators at low frequencies, and the rise of $\theta_{cal}(T)/\theta_{el}$ to a high-temperature limit which exceeds the Debye temperature implies a deficiency of oscillators at frequencies near $\omega_D$ and their presence at higher frequencies.
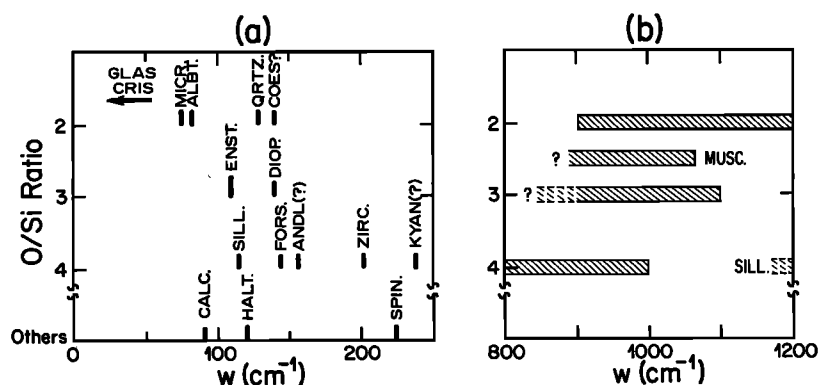
Evidence supporting these inferred deviations of silicate vi-

Fig. 5. Schematic diagram of the wave number of (a) the lowest and (b) the highest optical vibrations (measured at K = 0 by infrared, Raman, or inelastic neutron scattering data). Data on the lowest modes are taken from paper 2 and those on the highest modes from *Moenke* [1974, p. 112], *Lazarev* [1972], and paper 2.

brational spectra from the Debye model is available from spectroscopic measurements of lattice vibrational frequencies. (A detailed review of spectral data and new data on the minerals of interest in this study are given in paper 2. Only a brief introduction is given here.) Expressed in terms of wave numbers, elastic Debye 'frequencies' ($w = \omega_D/2\pi c$) of silicates range from about 200 cm$^{-1}$ to 600 cm$^{-1}$. Far-infrared data show optical modes at wave numbers as low as 75 cm$^{-1}$, and midinfrared and Raman data show that the vibrations extend to wave numbers in excess of 1000 cm$^{-1}$. Because no information on relative density of states is available for the modes at low wave numbers, it cannot be proved that they are in excess of the Debye distribution from the optical data alone; however, the high-frequency modes are clearly in excess of the Debye limit for most minerals. The positions of both the low- and the high-frequency modes are known to correlate with crystal structure (degree of polymerization of the SiO$_4^{-4}$ tetrahedra) in just the way required above to explain the calorimetric behavior observed.

Consider first the highest observed modes, in the range 900–1200 cm$^{-1}$ for silicates. It is well known that these are Si-O stretching modes and that the stretching modes lie at the highest frequencies for the framework silicates and at lower frequencies for the chain and orthosilicates [*Launer*, 1952]; the Al-O stretching modes are at ~700 cm$^{-1}$, at lower frequencies than the Si-O modes. These relations are summarized schematically in Figure 5a. The spectroscopic trends correspond to the calorimetric trends, which suggests that the high-temperature calorimetric behavior is controlled by the Si-O or Al-O stretching bonds. This will be demonstrated to be true in paper 3. Even the exceptions to the general trends of the high-temperature calorimetric behavior, notably zircon and sillimanite, are explicable in terms of known spectroscopic anomalies of the Si-O stretching bands. *White* [1975, p. 344] has shown that the main Raman-active Si-O stretching vibration in zircon is at anomalously high wave number (1008 cm$^{-1}$) in comparison to that of other orthosilicates (e.g., Raman bands at 828, 860, and 880 cm$^{-1}$ in olivine). *Lazarev* [1972, p. 171] and others (summarized in paper 2 of this series) have shown that the Si-O stretching frequencies in sillimanite are exceptionally high, among the highest known frequencies in any silicate. The apparently anomalous high-temperature limit for enstatite may be due to an ortho-clino transition at ~900°K [*Janaff*, 1965, 1966, 1967].

The dip in the $\theta_{cal}(T)/\theta_{el}$ curve at low temperature implies an excess heat capacity compared to that expected from the Debye model of a frequency spectrum and therefore implies

excess modes of vibration at low frequencies. Because the position of the dip and its magnitude are roughly correlated, one can state in a general way that the position of the modes is lowest and the number of excess modes greatest for the framework silicates and that the position is higher and the relative number less for the chain and orthosilicates. This corresponds to the systematic behavior observed in the far infrared and a few available Raman spectra (reported in paper 2). The correlation is shown schematically in Figure 5b. The frequency of the lowest optic vibrational modes at K = 0 is in the range 75–130 cm$^{-1}$ for the framework silicates, higher for the chain silicates (140–150 cm$^{-1}$), and highest for the orthosilicates (140–240 cm$^{-1}$). No information is available on the relative number of modes from spectroscopic data.

In a general way this discussion suggests that both the low-temperature and the high-temperature calorimetric behaviors are correlated with the degree of polymerization of the SiO$_4^{-4}$ tetrahedra. The spectroscopic characteristics are also correlated with the degree of polymerization of the tetrahedra and, in a qualitative way, suggest that the degree of deviation from a Debyelike vibrational spectrum depends on crystal structure. Any model for mineral heat capacities should be capable of explaining these general relations between the thermodynamic behavior and the structural properties.

### 3. CAUSES OF THE DEVIATIONS OF SILICATE HEAT CAPACITIES FROM DEBYE BEHAVIOR

The large variation of $\theta_{cal}(T)$ with temperature and its deviation from the value of $\theta_{el}$ are strong evidence that for most minerals the specific heat is predicted by the elastic Debye temperature only in a range of a few degrees Kelvin above absolute zero. Failure to meet conditions 1–4 enumerated in section 2 causes departures of the lattice spectrum from the simple parabolic form assumed by Debye. The assumptions of Debye theory are violated in at least four significant ways.

1. The assumption of a mean sound speed is not sufficient for minerals which show a significant degree of anisotropy (e.g., directional variations of more than 10% in the shear velocity).

2. The assumption of a constant velocity for all waves is not sufficient because the lattice waves show dispersion toward the Brillouin zone boundaries.

3. At low frequencies, optic vibrations in excess of the Debye spectrum may occur.

4. At high frequencies, optic vibrations may occur at frequencies much greater than those predicted by acoustic measurements.

The relative importance of these effects depends on the particular mineral and on the temperature range under consideration. In this section, simple models are used to demonstrate how each of these effects is a possible cause of the deviation of the heat capacity of silicates from the Debye model.

*Acoustic Modes of Vibration*

A real crystal differs from the elastic continuum assumed by Debye in the existence of a periodic lattice structure. Lattice waves are dispersive because the phase velocity depends on the frequency of the lattice vibrations; typically, the dispersion is strongest near the Brillouin zone boundaries, i.e., at short wavelengths. To illustrate the effects of the Brillouin zone boundaries, it is instructive to consider the vibrations of a simple monatomic chain lattice. This problem is treated in most elementary solid-state books [e.g., *Kittel*, 1968, p. 142]. Consider, for simplicity, waves which are purely longitudinal propagating in a monatomic chain in which the atoms are separated by distance $a$ (Figure 6a). Assume that Hooke's law is obeyed and that the force constant between two atoms separated from each other by $j$ lattice constants is $\phi_j$. (The $\phi_j$ will, in general, be different for longitudinal and transverse waves.) Then the force $F_r$ on atom $r$ due to the displacements of the atom $r + j$ is proportional to the difference of their displacements, $\mu_{r+j} - \mu_r$:

$$F_r = \sum_j \phi_j (\mu_{r+j} - \mu_r) \qquad (16)$$

The equation of motion of an atom of mass $m$ is therefore

$$m\frac{d^2\mu_r}{dt^2} = \sum_j \phi_j (\mu_{r+j} - \mu_r) \qquad -\infty < j < \infty \qquad (17)$$

Solutions to this equation have the form of a traveling wave,

$$\mu_r = \mu_r(0) \exp [iK(r + j)a - i\omega t] \qquad (18)$$

where $K$ (= $2\pi y$) is the wave vector and $\omega$ (= $2\pi\nu$) is the angular frequency.

For the special cases of central forces and nearest-neighbor interactions the frequencies of vibration are

$$\omega^2 = (2\phi_1/m)(1 - \cos Ka) \qquad (19)$$

or

$$\omega = (4\phi_1/m)^{1/2}|\sin (Ka/2)| \qquad (20)$$

The function $\omega(K)$ (or $\hbar\omega(K)$) is called the dispersion relation. In contrast to the Debye model, which assumes $\omega$ to be a linear function of $K$, the chain model shows that a lattice of discrete mass points gives rise to a periodic dependence of $\omega$ on $K$ (Figure 6b). Compared to a continuum model, $\omega$ is lowered near the boundaries of the lattice Brillouin zones, $K = \pm\pi/a$.

In the simplest model, in which a mean sound velocity is assumed, the effect of dispersion is to introduce a singularity into the frequency distribution at a cutoff frequency $\omega_m$ reduced from the Debye value $\omega_D$ (Figure 6c)
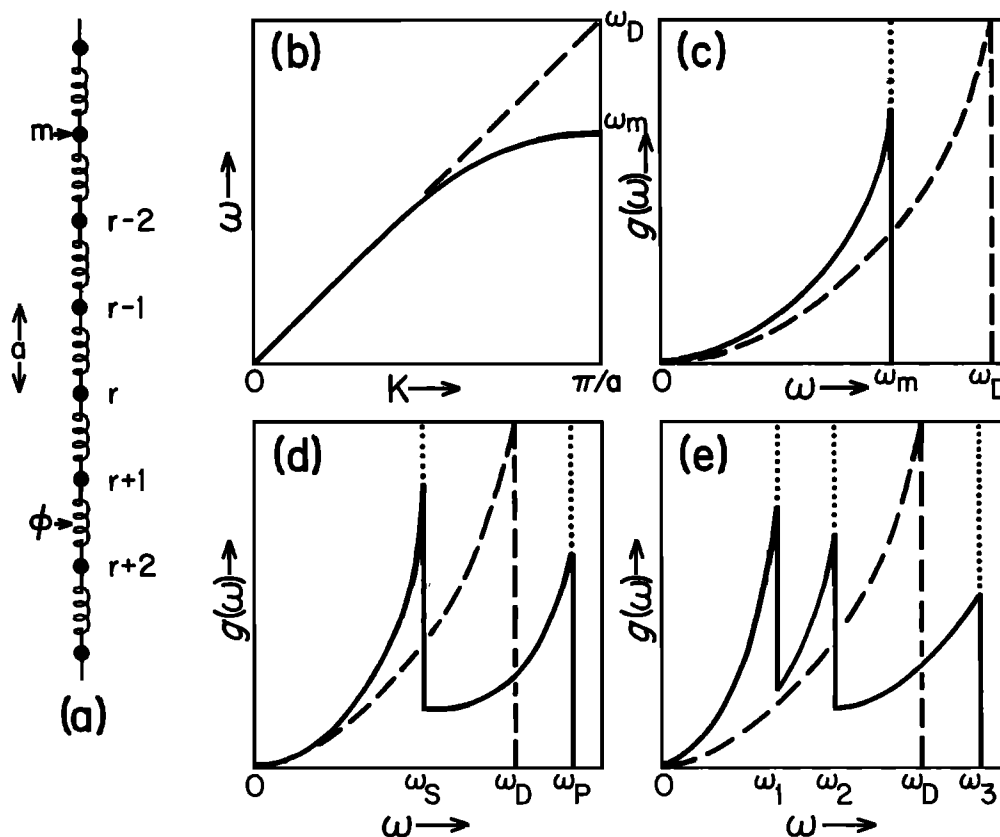


Fig. 6. (a) Linear monatomic chain. (b) Dispersion relation for monatomic chain (solid curve) compared to dispersion relation for Debye solid (dashed curve). (c) Vibrational spectrum of monatomic chain (solid curve) compared to Debye spectrum (dashed curve). (d) Vibrational spectrum of isotropic monatomic substance (solid curve), with separate $P$ and $S$ velocities, compared to Debye spectrum (dashed curve). (e) Vibrational spectrum of monatomic anisotropic solid (solid curve), with two shear velocities $v_1$ and $v_2$, compared to Debye spectrum (dashed curve).

$$\omega_m = \frac{\omega_D}{\pi/2} \approx \tfrac{2}{3}\, \omega_D \tag{21}$$

Dispersion laws for real solids are complicated functions of the magnitude and direction of **K**. However, it is a general requirement of the periodic lattice structure that the frequency be a periodic and continuous function of **K**, with the periodicity of the lattice Brillouin zones. In general, the frequency bends over from the linear relation observed as **K** approaches zero [Ziman, 1972, p. 36], and the dispersion relations observed in real solids are approximately represented by a sine function. Examples of measured and calculated dispersion curves for which this can be seen can be found as follows: $SiO_2$, quartz [Elcombe, 1967]; $TiO_2$, rutile [Traylor et al., 1971]; MgO [Borgonovi and Carriveau, 1968]; CsCl, CsBr, CsI [Karo and Hardy, 1968]; copper [Horton and Schiff, 1956]; and diamond [Blanchard and Varshni, 1967].

### Effect of Dispersion and Anisotropy on the Heat Capacity

The combined effects of dispersion and anisotropy of acoustic waves change the vibrational spectrum from that of a simple Debye model. Whereas the theoretical spectrum of an isotropic monatomic substance contains two acoustic branches, corresponding to transverse and longitudinal waves (Figure 6d), the theoretical spectrum of an anisotropic monatomic substance contains a third peak (Figure 6e) because the transverse velocities are, in general, not identical. Each of these waves is dispersed near the Brillouin zone boundaries. Therefore the combined effect of the anisotropy and dispersion is to introduce peaks into the frequency distribution $g(\omega)$ at frequencies $\omega_1$, $\omega_2$, and $\omega_3$ which are different from the Debye frequency computed on the basis of a mean sound speed (Figure 6e).

Because of anisotropy and dispersion the actual frequency distribution is a complicated function of frequency instead of a simple parabolic Debye spectrum. To represent an actual spectrum empirically, it is common practice [e.g., Barron and Morrison, 1957] to expand $g(\omega)$ in powers of $\omega^2$:

$$g(\omega) = a_2\omega^2 + a_4\omega^4 + a_6\omega^6 + \cdots \tag{22}$$

This series may be used for $\omega$ less the first singularity in $g(\omega)$. The equivalent Debye temperature $\theta_D$ at very low temperatures is then given by [Bhatia and Horton, 1955]

$$\theta_D = \theta_{el}\left[1 - \left(\frac{20\pi^2}{21}\right)\left(\frac{a_4}{a_2}\right)\left(\frac{kT}{\hbar}\right)^2 + \cdots\right] \tag{23}$$

The first term in this expansion gives the low-temperature Debye behavior. Since $a_2$ is always positive, it is clear that if $a_4$ is positive, $\theta_D$ will decrease if the temperature is increased above zero. The constant $a_4$ is positive for a monatomic sinusoidal dispersion law. If $a_4$ is positive, excess oscillators exist at low frequencies in violation of the Debye spectrum, causing a drop in $\theta_D$ with increasing temperature. If $a_4$ is negative, $\theta_D$ will first increase as the temperature increases. A discussion of the sign of $a_4$ with regard to elastic constants and crystal stability

$$\begin{vmatrix} m_1\omega^2 - \phi_1 - \phi_2 \\ \phi_1 \exp\,(-iKa) + \phi_2 \exp\,(iKa) \end{vmatrix}$$

for face-centered cubic minerals is given by Bhatia and Horton [1955]. The constant $a_2$ may be calculated from elastic wave data, but in general, it is not possible to calculate $a_4$ for complex substances such as minerals.

A comparison of mineral specific heat data with calculated models which take into account anisotropy and dispersion shows that although these two effects are significant at low temperatures, they cannot explain the abnormally large excess specific heat observed at low temperatures (Figure 4). This is partly because, as Leibfried [1955] pointed out, in a real substance with three acoustic branches the effects of anisotropy and dispersion in the acoustic branches are partially compensatory. Velocity anisotropy disperses the three spectral maxima associated with the shear and longitudinal velocities over a range of frequencies from $\omega_1 < \omega_D$ to $\omega_3 > \omega_D$ (see Figure 6e). Thus the two lowest shear modes may be 'compressed' below the mean Debye frequency, whereas the longitudinal mode is 'stretched' to a frequency higher than the Debye frequency. The effect of dispersion, however, is to add the $a_4$ term in (22) and effectively reduce the $\omega_3$ longitudinal peak back toward $\omega_D$. The net effect is a spectrum that leads to decreases in $\theta_{cal}(T)$ of the order of 0.1 of $\theta_{el}$, e.g., Pb in Figure 2. A second reason that anisotropy and dispersion cannot fully account for the observed behavior of $\theta_{cal}(T)$ of minerals is that the acoustic branches represent only a small fraction of the total modes. The majority of vibrational modes of complex minerals are optic modes and, as is demonstrated in paper 3, it is the behavior of these modes that causes most of the observed differences from Debyelike behavior.

### Optic Modes of Vibration

Vibrational properties common to complex lattices may be illustrated by considering a diatomic chain which has a basis of two masses $m_r = m_1$ and $m_{r+1} = m_2$ and two force constants $\phi_1$ and $\phi_2$ (Figure 7a). The larger mass will be designated as $m_1$, and the larger force constant as $\phi_1$; the interatomic distance will be designated $a$, so that $2a$ is the lattice repeat distance. The range of the first Brillouin zone is $-\pi/2a < K < \pi/2a$. The equations of motion of the atoms may be derived by a procedure similar to that discussed in the previous section for a monatomic chain. Under the assumption of nearest-neighbor interactions only, the equations of motion are

Particle $r$

$$F_r = \phi_1(\mu_{r+1} - \mu_r) + \phi_2(\mu_{r-1} - \mu_r) = m_1(d^2\mu_r/dt^2) \tag{24a}$$

Particle $r + 1$

$$F_{r+1} = \phi_1(\mu_r - \mu_{r+1}) + \phi_2(\mu_{r+2} - \mu_{r+1}) = m_2(d^2\mu_{r+1}/dt^2) \tag{24b}$$

Solutions to these equations have the form of traveling waves with different amplitudes (designated $\xi_1$ and $\xi_2$) on the even $(r, r + 2, \cdots)$ and odd $(r - 1, r + 1, \cdots)$ atoms:

$$\mu_r = \xi_2 \exp\,[irKa - i\omega t] \tag{25a}$$

$$\mu_{r+1} = \xi_1 \exp\,[i(r + 1)Ka - i\omega t] \tag{25b}$$

These equations have a solution only if the determinant of the coefficients of $\xi_1$ and $\xi_2$ vanishes:

$$\begin{vmatrix} \phi_1 \exp\,(iKa) + \phi_2 \exp\,(-iKa) \\ m_2\omega^2 - \phi_1 - \phi_2 \end{vmatrix} = 0 \tag{26}$$

This determinant is called the secular determinant.

Consider first the special case $\phi_1 = \phi_2 = \phi$. Kittel [1968, p. 149] has shown that for this case, two solutions exist for $\omega^2$ at all wave vectors $K$. For small $K$, these solutions are (Figure 7b)
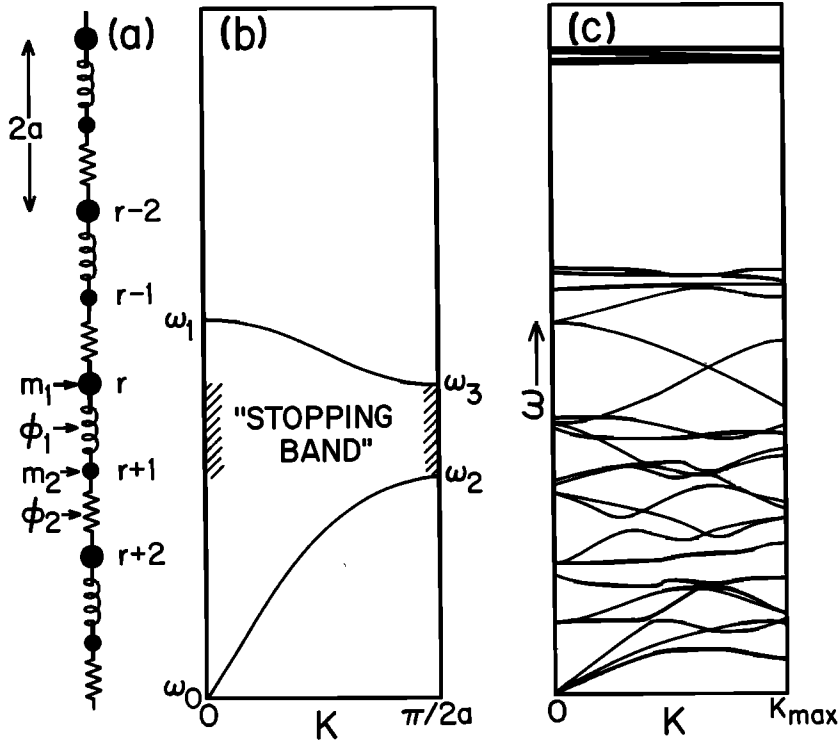
Fig. 7. (a) Linear diatomic chain with two different force constants. (b) Dispersion relation for the linear diatomic chain showing acoustic and optic branches and stopping band. (c) Dispersion relation for a complex substance, showing three acoustic branches and multiple optic branches. This sketch is from the measured dispersion relations for quartz of *Elcombe* [1967, p. 954].

Acoustic branch

$$\omega_0^2 \simeq 2\phi K^2 a^2/(m_1 + m_2) \qquad (27a)$$

Optic branch

$$\omega_1^2 \simeq 2\phi\left(\frac{1}{m_1} + \frac{1}{m_2}\right) \qquad (27b)$$

In the first solution (27a) to the secular determinant, $\omega$ approaches zero linearly as $K$ approaches zero. This behavior implies a constant group velocity $v = d\omega/dK$ of the waves. This is precisely the behavior of sound waves, and hence the name 'acoustic branch' is given to this solution.

In the second solution (27b) to the determinant, $\omega$ approaches a finite value as $K$ approaches zero. It can be demonstrated that at $K = 0$ the atoms vibrate in antiphase about a fixed center of mass. If the atoms under consideration carry opposite charges, the electric field of light waves will excite these lattice vibrations. For this reason, the second type of solution is called an 'optic branch' or 'optic mode.' Optic branches will exist for all crystals in which the atoms do not satisfy conditions 1-4 listed previously as requirements for a crystal to be 'essentially monatomic.'

Two solutions, which will be designated as $\omega_2$ and $\omega_3$, also exist at the Brillouin zone boundary, $K = \pm\pi/2a$ (Figure 7b). For equal force constants these solutions are

Acoustic branch

$$\omega_2 = (2\phi/m_1)^{1/2} \qquad (28a)$$

Optic branch

$$\omega_3 = (2\phi/m_2)^{1/2} \qquad (28b)$$

The ratio of optic to acoustic branch frequencies at the zone boundary is therefore $(m_1/m_2)^{1/2}$. Waves with frequencies less than $\omega_2$ and between $\omega_3$ and $\omega_1$ are propagated by the lattice. Such bands of frequencies are referred to as 'passing bands' [*Brillouin*, 1953]. Waves of frequencies outside these passing bands are not propagated but, rather, are attenuated. Such intervals as the one between $\omega_2$ and $\omega_3$ are referred to as 'stopping bands.' As the masses $m_1$ and $m_2$ become identical, the stopping band disappears and the optic branch becomes a continuation of the acoustic branch. However, it is folded back in $K$ space because the Brillouin zone is artificially reduced by the use of a unit cell of length $2a$; a zone of size $a$ is appropriate to the monatomic case.

For the general case of a lattice with different force constants and masses the determinant (26) has the solution

$$\omega^2 = \frac{(\phi_1 + \phi_2)}{2}\left(\frac{1}{m_1} + \frac{1}{m_2}\right) \pm \left\{\left(\frac{\phi_1 + \phi_2}{2}\right)^2\left(\frac{1}{m_1} + \frac{1}{m_2}\right)^2\right.$$
$$\left. - 4\frac{\phi_1\phi_2}{m_1 m_2}\sin^2 Ka\right\}^{1/2} \qquad (29)$$

These solutions are shown in Figure 8. For small $K$, $\sin^2 Ka \simeq K^2 a^2$, and (29) has the two roots

Acoustic branch

$$\omega_0^2 \simeq (\phi_1 + \phi_2)(m_1 + m_2)^{-1}K^2 a^2 \qquad (30a)$$

Optic branch

$$\omega_1^2 \simeq (\phi_1 + \phi_2)\left(\frac{1}{m_1} + \frac{1}{m_2}\right) \qquad (30b)$$

At the Brillouin zone boundaries, $K = \pm\pi/2a$, the branches approach limits determined by both the mass ratio $m_1/m_2$ and the force constant ratio $\phi_1/\phi_2$. If $\phi_1 \gg \phi_2$, the two branches approach the limits
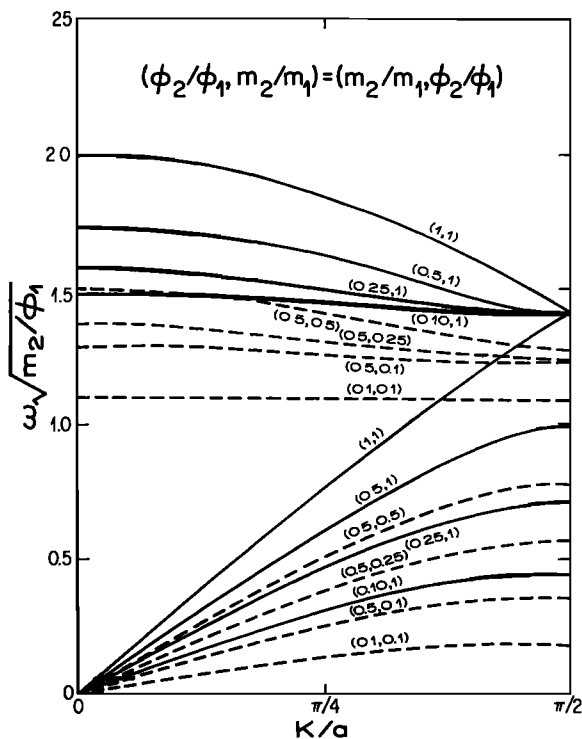
Fig. 8. Generalized dispersion relations for a linear diatomic chain with two different force constants. Numbers shown in parentheses with the curves refer to the ratios $\phi_2/\phi_1$ and $m_2/m_1$.

Acoustic branch

$$\omega_2{}^2 \simeq \frac{4\phi_2}{(1 + \phi_2/\phi_1)(m_1 + m_2)} \qquad (31a)$$

Optic branch

$$\omega_3{}^2 \simeq \phi_1(1 + \phi_2/\phi_1)\left(\frac{1}{m_1} + \frac{1}{m_2}\right) \qquad (31b)$$

In the case $m_1 = m_2$, then, the ratio of frequencies at the Brillouin zone boundary for the optic and acoustic branches is $(\phi_1/\phi_2)^{1/2}$.

From the simple examples of monatomic and diatomic chains, several features can be recognized which hold for polyatomic, three-dimensional lattices [Brillouin, 1953, p. 24; Born and Huang, 1954].

1. The frequency $\omega$ is a periodic function of the wave vector $\mathbf{K}$.

2. If the primitive unit cell of the one-dimensional lattice contains $n$ degrees of freedom, there will be $n$ different dispersion curves. By analogy, if the primitive unit cell of a three-dimensional lattice contains $n$ particles, it has $3n$ degrees of freedom, and there will be $3n$ different waves corresponding to each $\mathbf{K}$ value (a schematic example, based on data for quartz, is shown in Figure 7c).

3. Waves with frequencies in the range of the dispersion curves (e.g., between $\omega_0 = 0$ and $\omega_2$ and between $\omega_1$ and $\omega_3$ for the diatomic case (Figure 6b)) are propagated by the lattice. These ranges of frequencies are called passing bands [Brillouin, 1953, p. 25]. The number of passing bands equals the number of degrees of freedom in the unit cell (with possible overlapping of passing bands).

4. Frequencies outside the passing bands are not propagated through the lattice. Such frequency ranges, e.g., between $\omega_2$ and $\omega_3$ in Figure 6b, are called stopping bands.

The failure of the Debye model to take into account such detailed spectral features of complex crystals as anisotropy, mass differences, and force constant differences is responsible in a general way for its failure when it is applied to complex crystals. If minerals were simple diatomic substances, it might be reasonable to pursue simple chain models further to obtain estimates of dispersion relations and vibrational spectra. However, a description of the vibrational spectrum of a lattice requires detailed knowledge of local interatomic forces. Lattice dynamical models have not, in general, been successful for complex, polyatomic, anisotropic minerals. A complete lattice dynamics formulation requires knowledge of more lattice force constants than are generally available for minerals and results in an immense number of coupled differential equations which would be quite unreasonable to solve for most minerals of geological and geophysical interest. However, several results of lattice dynamics theory are of use in the formulation of a simplified generalized model and these will be the basis of the model proposed in paper 3 of this series.

As was mentioned previously, spectroscopic data (presented briefly in paper 2) demonstrate that optic vibrational modes occur at both very low and very high frequencies compared to typical Debye frequencies obtained from acoustic data. In the next section, simple models are developed to estimate the effect which these modes have on the heat capacity.

*Effect of Low-Frequency Optic Modes on the Heat Capacity*

The effect on $\theta_{cal}(T)$ of a vibrational spectrum with dispersion, a stopping band, and a single low-frequency or high-frequency optic mode can be understood by examining the simple models illustrated in Figure 9, in which characteristic dispersion and frequency distribution curves for the simple diatomic model discussed in the previous section are compared with the single curve of the Debye model (dashed curve). Consider first the case in which an optic mode is below the Debye frequency and has so little dispersion that it can be represented by an Einstein oscillator (Figure 9a) $\omega_1 = \omega_3 < \omega_D$. The frequency distribution corresponding to this model is shown in Figure 9b. The dashed curve represents a Debye spectrum with the coefficient $a$ determined by the acoustic velocities according to (6). The area under the Debye curve is $3N = 3nN_A$, the total number of degrees of freedom of the vibrational oscillators in the crystal. The solid curve representing the vibrational spectrum of the diatomic solid is comprised of two parts: a low-frequency acoustic distribution, modified by a sinusoidal dispersion relation (as in (23) and (33)), and a higher-frequency optic distribution. The total number of degrees of freedom of the oscillators in this modified distribution is also equal to $3N$. It is evident that owing to dispersion and to the low-frequency position of the optic mode, many modes of vibration occur in excess of the Debye spectrum at frequencies $\omega$ less than the Debye frequency $\omega_D$. At extremely low temperatures, where only the acoustic branch contributes to the heat capacity, the specific heat is that of the pure Debye model and $\theta_{cal} = \theta_D$. As the temperature rises to $T \sim \hbar\omega_2/k$, the extra contribution from the excess oscillators due to dispersion at the zone boundary begins to be felt; i.e., the contribution of the term containing $a_4$ in (23) becomes appreciable. Similarly, as the temperature rises to $T \sim \hbar\omega_1/k$, the extra contribution to the heat capacity from the low-frequency optic branch becomes appreciable. The dispersion relation and the low-frequency optic branch both contribute excess specific heat in comparison to the Debye model. Hence when $\theta_{cal}(T)$ is eval-
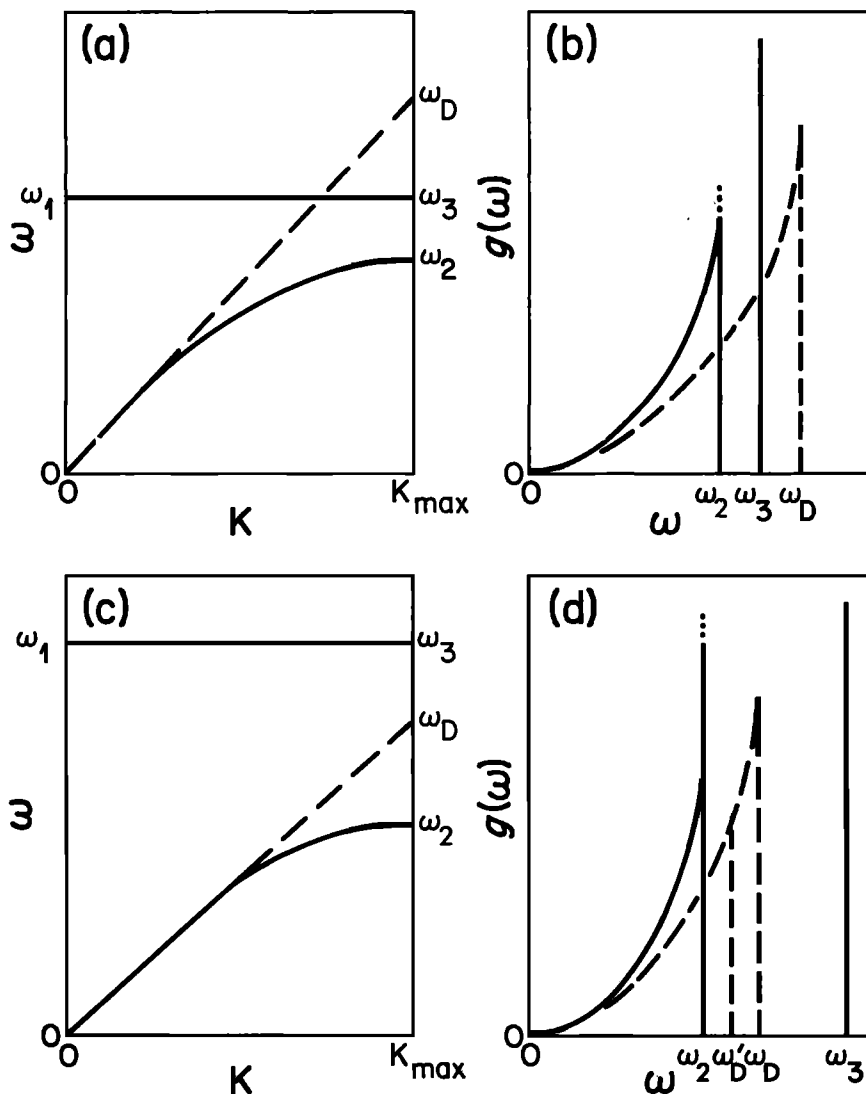
Fig. 9. (a) Simplified dispersion relations for a diatomic solid (solid curves) compared to the Debye spectrum (dashed curve). The acoustic branch is periodic in $K$; the optic branch is flat, $\omega_1 = \omega_3$, and is at a low frequency relative to $\omega_D$. (b) Vibrational spectrum corresponding to the dispersion relations in Figure 9a. (c) Dispersion relations for a diatomic solid (solid curves) compared to a Debye spectrum (dashed curve). The acoustic branch is periodic in $K$; the optic branch is flat, $\omega_1 = \omega_3$, and is at high frequency relative to $\omega_D$. (d) Vibrational spectra $g(\omega)$ corresponding to the dispersion relations in Figure 9c.

uated by replacing $\theta_D$ in (14) with $\theta_{cal}(T)$ chosen so as to reproduce the actual $C_V$, the $\theta_{cal}(T)$ so determined drops below $\theta_{el}$, since $C_V(\theta_D/T)$ is a monotonically decreasing function of $\theta_D/T$.

The few low-temperature data available for glass, quartz, cristobalite, coesite, stishovite, rutile, calcite, and the $Al_2SiO_5$ polymorphs show that the measured $\theta_{cal}(T)$ curves decrease rapidly from $\theta_{el}$ to a minimum in the region 0.01–0.05 of $\theta_{el}$. This decrease in $\theta_{cal}(T)$ could be explained by the presence of a single low-frequency Einstein oscillator, as discussed above, but such a simple model would not account for the subsequent rise of $\theta_{cal}(T)$ above $\theta_{el}$ at higher temperatures (see Figures 3 and 4). This rise is due to vibrations, such as the Si-O stretching mode, at frequencies higher than the Debye frequency. In the next section the effect of such modes is discussed.

*Effect of High-Frequency Optic Modes on the Heat Capacity*

The effect on $\theta_{cal}(T)$ of a vibration spectrum with high-frequency optic oscillators can be understood from the simple

model illustrated in Figures 9c and 9d. In this model the optic mode, assumed to be flat, is separated from the acoustic modes by a substantial stopping band, so that $\omega_1 = \omega_3 > \omega_D$. As for the previous example the dashed curve represents a Debye spectrum with the coefficient $a$ determined by the acoustic velocities according to (6). The solid curve is comprised of two parts: some of the vibrations of the Debye spectrum have been shifted to a higher frequency $\omega_3 = \omega_E$, leaving the lowest-frequency part of the Debyelike spectrum unchanged. This has been done by the arbitrary procedure of cutting off the Debyelike spectrum sharply at a frequency lower than the original cutoff frequency $\omega_D$ for the pure Debye spectrum. The effect of dispersion of the acoustic branch will be ignored for the purpose of this discussion. The area under the original curve is $3N = 3nN_A$, the total number of degrees of freedom in the crystal; the number of oscillators retained in the Debyelike, acoustic portion of the modified spectrum is designated by $3N' = 3n'N_A$ (and correspondingly, $n' = N'/N_A$). The ratio $n'/n$ is the fractional part of the spectrum, which is retained in the acoustic branch; and from (9) it follows that

$$\omega_D' = (n'/n)^{1/3}\omega_D \qquad (32)$$

At low temperatures, when only the lowest-frequency oscillators contribute to the specific heat, the calorimetric behavior is unchanged from that of the pure Debye model, and the Debye temperature is $\theta_{cal} = \theta_D$, as given by (10). As the temperature rises to $T \sim \theta_D'$, where $\theta_D'$ is given by (10) with $\omega_D$ replaced by $\omega_D'$, the lack of oscillators immediately above $\omega_D'$ begins to be sensed in the thermal behavior. The specific heat begins to fall below what it would be if these oscillators were not missing. Hence $\theta_{cal}(T)$ rises above $\theta_D$.

Assume for the moment that $\omega_E$ lies high enough that the contributions of the remaining oscillators do not begin to be felt yet at the temperature $T \sim \theta_D'$. (A good rule of thumb is that an oscillator of wave number $w = \omega/2\pi c$ contributes substantially when $T$, in degrees Kelvin, is numerically equal to $w$, in cm$^{-1}$.) Then $C_V$ is actually given by (14) with $\theta_D$ replaced by $\theta_D'$. However, this does not imply that there will be a close relation between the 'curtailed Debye temperature' $\theta_D'$ (which is lower than $\theta_D$) and the $\theta_{cal}(T)$ that is actually found (which is higher than $\theta_D$): this is because in calculating $C_V$ from (14) we must also replace $n$ by $n'$, whereas $\theta_{cal}(T)$ is evaluated by using $n$. At high temperature, $D(\theta_D/T)$ approaches $3R$; hence in this intermediate temperature range where the oscillators at $\omega_E$ are not yet felt, $\theta_{cal}(T)$ is given by the solution of

$$nD(\theta_{cal}(T)/T) = 3Rn' \qquad (33)$$

which is

$$\theta_{cal}(T) = TD^{-1}(3Rn'/n) \qquad (34)$$

where $D^{-1}(x)$ represents the inverse Debye function. Under the assumptions made, $\theta_{cal}$ will thus increase linearly with $T$ for $T \gtrsim \theta_D'$, the rate of increase being greater the smaller the acoustic spectral fraction $n'/n$. (For $n'/n = \frac{1}{3}$, $D^{-1}(3Rn'/n) = 4.25$.)

At a high temperature $T \sim \hbar\omega_1/k$ the contribution from the oscillators at $\omega_E$ stabilizes the rise in $\theta_{cal}(T)$ at a level $\theta_{cal} \sim \theta_E$. To determine the actual asymptotic value $\theta_{cal}(\infty)$ reached, the high-temperature asymptotic forms of the Debye and Einstein functions are utilized:

$$D\left(\frac{\theta_D}{T}\right) = 3R\left[1 - \frac{1}{20}\left(\frac{\theta_D}{T}\right)^2 + \cdots\right] \qquad (35)$$

$$E\left(\frac{\theta_E}{T}\right) = 3R\left[1 - \frac{1}{12}\left(\frac{\theta_E}{T}\right)^2 + \cdots\right] \qquad (36)$$

Applying the definition of $\theta_{cal}(T)$ given previously, we have

$$nD\left(\frac{\theta_{cal}}{T}\right) = n'D\left(\frac{\theta_D'}{T}\right) + (n - n')E\left(\frac{\theta_E}{T}\right) \qquad (37)$$

In the high temperature limit this becomes

$$3Rn\left[1 - \frac{1}{20}\left(\frac{\theta_{cal}(\infty)}{T}\right)^2\right] = 3Rn'\left[1 - \frac{1}{20}\left(\frac{\theta_D'}{T}\right)^2\right]$$
$$+ 3R(n - n')\left[1 - \frac{1}{12}\left(\frac{\theta_E}{T}\right)^2\right] \qquad (38)$$

which gives, with the help of $\theta_D' = (n'/n)^{1/3}\theta_D$

$$\theta_{cal}^2(\infty) = (n'/n)^{5/3}\theta_D^2 + \tfrac{5}{3}[1 - (n'/n)]\theta_E^2 \qquad (39)$$

This equation was derived for the restricted case $n'/n = \frac{1}{2}$ by Lord [1941] in calculations of the contribution of translational and rotational modes of molecular lattices to the specific heat. Equation (39) allows us to see how the limiting $\theta_{cal}(\infty)$ depends on the oscillator partitioning fraction $n'/n$ and on $\theta_E$. It can be shown that if $\theta_E > \theta_D$ and $0 < n'/n < 1$,

$$\theta_D < \theta_{cal}(\infty) < (\tfrac{5}{3})^{1/2}\theta_E \qquad (40)$$

In principle, molecular crystals should provide the most striking examples of this model, but in practice, $\omega_E$ is so much greater than $\omega_D'$ that these crystals usually melt or dissociate before the contributions of the intramolecular vibrations at $\omega_E$ to $C_V$ become appreciable. For such crystals it is obvious that the vibrational unit for the acoustic vibrations should be chosen as the whole molecule rather than the individual atom. In spite of the fact that the molecule is polyatomic, one would take both $n = 1$ and $n' = 1$, and one would then expect to find the $\theta_{cal}(T)$ calculated on this basis to be approximately constant if the intermolecular (translational and librational) vibrations follow a Debyelike spectrum. Lord [1941] discussed the likely intermolecular spectrum of molecular crystals, and the reader is referred there for detailed discussion.

A model such as the one discussed here might be applied to silicates with the assumption that the Si-O stretching vibrations can be represented as an Einstein oscillator. With this assumption, $n'/n \simeq 0.8$ (paper 2), $\theta_D \simeq 600°$, and $\theta_E \simeq 1500°$ (corresponding to an Einstein oscillator at 1050 cm$^{-1}$). Equation (39) then gives $\theta_{cal}(\infty) \sim 1000°$ and $\theta_D' \sim 0.93 \times \theta_D \sim 550°$ (corresponding to a truncation of the Debye spectrum at $w_D' = 375$ cm$^{-1}$). Measured $\theta_{cal}(\infty)$ values for silicates are in fact between 1200°K (for some framework silicates) and 950° (for orthosilicates) (see Figures 3 and 4). The $\theta_{cal}(\infty)$ values for spinel, rutile, and stishovite, also shown in these figures, are lower than those for the SiO$_4^{-4}$ silicates, reflecting vibrational bands in the region 700-800, 400-800, and 800-900 cm$^{-1}$, respectively.

The agreement between calculated and observed high-temperature limits suggests that the addition of a high-frequency Einstein oscillator to represent the Si-O tetrahedral stretching vibrations (or, in a few cases, Al-O, Si-O, or Ti-O octahedral vibrations) might be a reasonable approximation to the true vibrational spectrum at high frequencies. However, attempts which have been made to represent optic modes of silicates by a simple model with a single weighted Einstein function supplementing a truncated Debye distribution were of limited success [Blackman, 1955]. This is simply because a model with a Debye spectrum supplemented by a single Einstein function cannot account for both the decrease in $\theta_{cal}(T)$ at low temperatures and the subsequent rise in $\theta_{cal}(T)$ at high temperatures. A more realistic estimate of the distribution of oscillators in the wave number range 100-1200 cm$^{-1}$ must be made in order to calculate the thermodynamic functions; this estimate is the subject of paper 3.

## 4. Summary

The measured heat capacities of minerals show strong deviations from Debyelike calorimetric behavior at all temperatures above a few degrees Kelvin. The deviations vary systematically with crystal structure. The Debye model does not account for the measured calorimetric properties of minerals because it does not allow for anisotropy of elastic parameters, dispersion of lattice waves at Brillouin zone boundaries, and low and high frequency modes arising from optic vibrations. In paper 2 of this series, characteristics of optic vibrations of minerals as known from infrared, Raman, and neutron scattering data are discussed. In paper 3 a simple model based on generalized vibrational characteristics is developed to replace the Debye

model for calculations of thermodynamic properties of minerals.

## APPENDIX: SCHEME FOR ESTIMATING DIRECTIONALLY AVERAGED SHEAR AND LONGITUDINAL VELOCITIES

Because there are few data on directionally averaged wave velocities for minerals, it is necessary to estimate these velocities (which will be used in the model in paper 3). Denote by $u_i$ the directional average

$$u_i \equiv \left[ \frac{1}{4\pi} \int_\Omega \frac{d\Omega}{v_i{}^3(\theta, \phi)} \right]^{-1/3} \quad (A1)$$

where $i = 1$ and $i = 2$ apply to the directionally averaged slow and fast shear velocities, respectively, and $i = 3$ applies to the directionally averaged longitudinal velocity. I assume that

$$u_3 = v_{\text{VRH},P} \quad (A2)$$

*Robie and Edwards* [1966] have shown that this is a good assumption in the cases of rutile and calcite.

It is much more difficult to specify two characteristic shear velocities because the only data commonly available for minerals are single VRH shear velocities $v_{\text{VRH},S}$. In order to make use of these data, I assume that

$$\frac{1}{u_1{}^3} + \frac{1}{u_2{}^3} = \frac{2}{v_{\text{VRH},S}{}^3} \quad (A3)$$

and further assume that the $u_1$ and $u_2$ which satisfy this relation

are representative of spatially averaged slow and fast shear velocities. Equations (A2) and (A3) assure that $\theta_{\text{el}}$ calculated by (7) and (11) is approximately equal to the value obtained from polycrystalline elastic constants. However, since infinite combinations of $u_1$ and $u_2$ could satisfy (A3), either $u_1$ or $u_2$ must be separately specified. I assume that either the slow or the fast shear wave velocity can be estimated if single-crystal acoustic velocity measurements in high-symmetry directions have been published for the mineral under consideration. Measurements in high-symmetry directions give minimum and maximum shear wave velocities [e.g., *Robie and Edwards*, 1966]. It would be convenient if these measured minimum and maximum values could be used as representative averages $u_1$ and $u_2$; however, the velocities in high-symmetry directions are generally maxima or minima of a smoothly varying directional velocity function and are thus not representative of an averaged value but rather of extrema [e.g., *Robie and Edwards*, 1966]. It can be demonstrated that they do not represent directionally averaged values by the following argument: The requirement that $u_2$ be finite places a restriction on $u_1$ through (A3):

$$u_1 > v_{\text{VRH},S}/2^{1/3} \gtrsim 0.8 v_{\text{VRH},S} \quad (A4)$$

The experimental data show, however, that the minimum shear velocity measured in a high-symmetry direction may be considerably less than $0.8 v_{\text{VRH},S}$. Therefore it must be smaller than the directionally averaged minimum value. For example,

TABLE A1. Directionally Averaged Velocities From Single-Crystal Maximum and Minimum Velocities and VRH Velocities

| Mineral | $v_{\text{VRH},P}$ (1) | $v_{\text{VRH},S}$ (2) | $v_{\text{min},S}$ (3) | $v_{\text{max},S}$ (4) | From (A5) and (A6) $u_1$ | From (A5) and (A6) $u_2$ | From (A7) and (A6) $u_1$ | From (A7) and (A6) $u_2$ | From (A8) and (A6) $u_1$ | From (A8) and (A6) $u_2$ | From (A9) and (A6) $u_1$ | From (A9) and (A6) $u_2$ | References |
|---|---|---|---|---|---|---|---|---|---|---|---|---|---|
| Halite | 4.56 | 2.61 | 2.43 | 2.91 | 2.50 | 2.74 | 2.52 | 2.71 | 2.52 | 2.70 | 2.49 | 2.76 | 1, 2, SW 11844; 3, 4, calculated from elastic constants, SW 11844 |
| Periclase | 9.71 | 6.05 | 5.31 | 6.60 | 5.83 | 6.30 | 5.62 | 6.62 | 5.68 | 6.53 | 5.80 | 6.34 | 1, 2, SW 10928; 3, 4, *Spetzler* [1970] |
| Quartz | 6.02 | 4.05 | 3.30 | 5.11 | 3.76 | 4.46 | 3.60 | 4.88 | 3.68 | 4.65 | 3.70 | 4.58 | 1, 2, SW 62894; 3, 4, *McSkimmin et al.* [1965] |
| Coesite | 8.19 | 4.59 | 8.54 | (6.60) | 4.17 | 5.24 | 3.93 | 6.17 | 4.06 | 5.56 | 4.05 | 5.60 | 1–4, *Weidner and Carleton* [1977] |
| Rutile | 9.26 | 5.14 | 3.31 | 6.76 | 4.73 | 5.73 | | | 4.22 | 8.78 | 4.64 | 5.95 | 1, 2, SW 22229; 3, 4, *Manghnani* [1969] |
| Microcline | 6.02 | 3.34 | 2.14 | 4.96 | 3.02 | 3.85 | | | 2.74 | 5.81 | 2.93 | 4.15 | 1, 2, SW 42404; 3, 4, *Alexandrov and Ryzhova* [1962] |
| Albite (9% An) | 6.06 | 3.33 | 2.56 | 5.45 | 2.98 | 3.91 | 2.84 | 4.52 | 2.95 | 4.05 | 2.87 | 4.39 | 1, 2, SW 42406; 3, 4, *Ryzhova* [1964] |
| Spinel | 9.82 | 5.62 | 4.19 | 6.54 | 5.31 | 6.00 | 4.70 | 8.44 | 4.90 | 7.09 | 5.26 | 6.08 | 1, 2, SW 11876; 3, 4, *Lewis* [1966] |
| Diopside | 7.70 | 4.38 | 3.94 | 4.83 | 4.21 | 4.58 | 4.13 | 4.69 | 4.16 | 4.65 | 4.19 | 4.61 | 1, 2, SW 42397; 3, 4, *Alexandrov et al.* [1964] |
| Enstatite | 7.85 | 4.76 | 4.27 | 4.99 | 4.69 | 4.86 | 3.60 | 4.88 | 3.68 | 4.65 | 3.70 | 4.58 | 1–4, *Kumazawa*, [1969] |
| Forsterite | 8.56 | 4.93 | 4.42 | 5.00 | 4.90 | 4.96 | 4.64 | 5.29 | 4.68 | 5.24 | 4.89 | 4.97 | 1–4, *Verma* [1960] (Voigt average) |
| Zircon | 8.06 | 3.97 | 2.94 | 4.87 | 3.71 | 4.33 | 3.30 | 6.14 | 3.46 | 5.05 | 3.66 | 4.42 | 1, 2, SW 22252; 3, 4, *Ryzhova et al.* [1966] |
| Calcite | 6.53 | 3.23 | 2.59 | 4.71 | 2.93 | 3.70 | 2.84 | 3.98 | 2.91 | 3.76 | 2.84 | 3.97 | 1, 2, SW 62845; 3, 4, *Pesselnick and Robie* [1963] |
| Corundum | 10.85 | 6.35 | 5.75 | 6.91 | 6.12 | 6.59 | 6.01 | 6.75 | 6.05 | 6.70 | 6.10 | 6.63 | 1, 2, SW 62813; 3, 4, *Bernstein* [1963] |

All velocities are in kilometers per second. Values of $u_1$ and $u_2$ from (A5) and (A6) are used in the model of paper 3. Blank entries indicate that $u_1 < 0.8 v_{\text{VRH},S}$; therefore $u_2$ cannot be calculated because (A7) and (A6) do not have a solution. SW means *Simmons and Wang* [1971]; code numbers are given.

for microcline, $v_{VRH,S} = 3.34$ km/s ($0.8v_{VRH,S} = 2.67$ km/s), but the minimum measured shear velocity is only 2.14 km/s [Alexandrov and Ryzhova, 1962]. Thus velocities measured in high-symmetry directions are not suitable choices for $u_1$ and $u_2$ because (A4) is violated and, in general, (A3) would not be satisfied.

Many schemes to estimate $u_1$ and $u_2$ could be devised; four which represent extreme cases are discussed here. Consider first the case where the maximum and minimum shear wave velocities $v_{max,S}$ and $v_{min,S}$ are known in high-symmetry directions. The velocity $u_2$ can be estimated by requiring

$$\frac{2}{u_2^3} = \frac{1}{v_{VRH,S}^3} + \frac{1}{v_{max,S}^3} \tag{A5}$$

Then $u_1$ follows from the requirement that

$$\frac{1}{u_1^3} + \frac{1}{u_2^3} = \frac{2}{v_{VRH,S}^3} \tag{A6}$$

Alternatively, $u_1$ could first be determined by requiring that

$$\frac{2}{u_1^3} = \frac{1}{v_{VRH,S}^3} + \frac{1}{v_{min,S}^3} \tag{A7}$$

with $u_2$ following from the requirement of (A6).

A third possibility is a linear averaging scheme

$$u_1 = (v_{min} + v_{VRH,S})/2 \tag{A8}$$

with $u_2$ determined from (A5) or, correspondingly,

$$u_2 = (v_{max} + v_{VRH,S})/2 \tag{A9}$$

with $u_1$ determined from (A5).

Velocities $u_1$ and $u_2$ from these four averaging schemes are shown in Table A1. Because the velocity $u_1$ is constrained through (A4) to values between $v_{VRH,S}/2^{1/3}$ and $v_{VRH,S}$, its value is not highly dependent on the averaging scheme used, and variations in $u_1$ are generally less than 10%. Note, however, that for highly anisotropic minerals the averaging scheme represented by (A7) and (A6) leads to a solution for $u_1$ which violates (A4) and therefore cannot be used. Somewhat larger variations may be obtained for the value of $u_2$ because it is unconstrained and, mathematically, could become very large as $u_1$ approaches $v_{VRH,S}/2^{1/3}$. The values given by (A5) and (A6) are used in the model of paper 3. The uncertainty introduced into $C_V$ calculations from the lack of a rigorous averaging procedure for $u_1$ is generally small and apparent only at very low (a few degrees) temperatures because the acoustic modes comprise a relatively small fraction of the total modes.

For those materials for which single-crystal velocities have not been measured but for which polycrystalline VRH averages are available I have estimated $u_1$ by assuming that the ratio $u_1/v_{VRH,S}$ is the same as that for structurally similar materials, e.g., for stishovite using rutile; for coesite using quartz (or microcline); and for orthosilicates kyanite and andalusite using olivine and zircon. The velocity $u_2$ is then calculated from (A6).

According to these choices, $\theta_{el}$ is given by (7) and (11) as

$$\theta_D = \frac{\hbar}{k} \left(\frac{18\pi^2 n N_A}{ZV}\right)^{1/3} \left(\frac{1}{u_1^3} + \frac{1}{u_2^3} + \frac{1}{u_3^3}\right)^{-1/3} \tag{A10}$$

## NOTATION

Equation numbers given refer to the first use of the symbol in an equation or to the equations nearest its first occurrence in text.

| | |
|---|---|
| $\mathbf{a_1, a_2, a_3}$ | basic vectors of the primitive lattice, (1). |
| $a$ | interatomic distance, (18). |
| $a$ | coefficient of the Debye distribution function $g(\omega)$, (4) and (5). |
| $a_P, a_S$ | coefficients of Debyelike spectrum with separate longitudinal ($P$) and shear ($S$) branches, between (5) and (6). |
| $a_2, a_4, a_6, \cdots$ | coefficients in the expansion of $g(\omega)$ in powers of $\omega^2$, (23). |
| $A$ | general amplitude coefficient, between (2) and (3). |
| $\mathbf{b_1, b_2, b_3}$ | reciprocal basis vectors, (1). |
| $c$ | speed of light. |
| $C_V$ | molar heat capacity, (13) and Table 1. |
| $C_V^E$ | heat capacity of an Einstein oscillator (same as $E(\hbar\omega/kT)$), (12). |
| $d$ | density of wave vectors in reciprocal space, before (4). |
| $D(\hbar\omega_D/kT), D(\theta_D/T)$ | Debye heat capacity function, (14). |
| $D(\theta_D/T)$ | derivative of the Debye function, Table 2. |
| $f(K)$ | density of vibrational states in reciprocal space, before (4). |
| $E$ | internal energy (molar), Table 1. |
| $\mathcal{E}(\hbar\omega/kT)$ | Einstein heat capacity function, (12b). |
| $F$ | Helmholtz free energy (molar), Table 1. |
| $F_r$ | force on atom $r$, (16). |
| $g(K), g(\omega)$ | frequency distribution function, (4). |
| $h,$ | Planck constant, equal to $6.625 \times 10^{-27}$ ergs s. |
| $\hbar$ | Planck constant divided by $2\pi$. |
| $k$ | Boltzmann constant, equal to $1.380 \times 10^{-16}$ ergs deg$^{-1}$. |
| $\mathbf{K}(\eta)$ | wave vector, (2). |
| $\mathbf{K_{max}}$ | maximum wave vector (Brillouin zone boundary), (8). |
| $m, m_i$ | particle mass, (17). |
| $N$ | Number of atoms (oscillators) in the crystal, equal to $nN_A$, between (5) and (6). |
| $N'$ | number of oscillators in a truncated Debye spectrum, (32). |
| $N_A$ | Avogadro's number, equal to $6.023 \times 10^{23}$ mol$^{-1}$, between (5) and (6). |
| $n$ | number of atoms in the chemical formula on which the molar volume is defined, between (5) and (6). |
| $n'$ | fractional number of formula unit oscillators in a truncated or modified Debye spectrum, equal to $N'/N_A$, (32). |
| $n'/n$ | acoustic spectral fraction. |
| $\hat{n}$ | unit direction vector, between (2) and (3). |
| $R$ | gas constant per mole, equal to 1.988 cal mol$^{-1}$ deg$^{-1}$. |
| $S$ | entropy (molar), Table 1. |
| $t$ | time, between (2) and (3). |
| $T$ | temperature, degrees Kelvin unless otherwise indicated. |
| $u_{1,2,3}$ | directionally averaged acoustic velocity (A1). |

$v(\theta, \phi)$ acoustic velocity, (3).

$v_m$ mean sound speed, (7).

$v_p$ acoustic longitudinal wave velocity, (6).

$v_S$ acoustic shear wave velocity, (6).

$v_1$ acoustic velocity of the lowest shear branch, (6).

$v_2$ acoustic velocity of the highest shear branch, (6).

$v_3$ acoustic velocity of the longitudinal branch, (6).

$v_{VRH,P}$ Voigt-Reuss-Hill acoustic velocity for longitudinal branch, (7).

$v_{VRH,S}$ Voigt-Reuss-Hill acoustic velocity for shear branch, (7).

$V$ molar volume, between (5) and (6).

$V_L$ volume of primitive unit cell, (2).

$V_R$ volume of unit cell of reciprocal lattice (Brillouin zone), (2).

$w$ wave number, equal to $\omega/2\pi c$ cm$^{-1}$, before (16).

$x$ general displacement vector, between (2) and (3).

$x$ dimensionless frequency, equal to $\hbar\omega/kT$, (14).

$y(\eta), y$ reciprocal lattice vector, equal to $K/2\pi$, (3).

$Z$ partition function Table 1.

$\beta$ atomic potential energy, Table 1 only.

$\delta$ phase factor, between (2) and (3).

$\eta_1, \eta_2, \eta_3$ coefficients of scalar components of wave vector, (2).

$\theta_D$ Debye temperature, (10).

$\theta_D'$ curtailed Debye temperature of truncated Debye spectrum, after (32).

$\theta_E$ Einstein temperature, (36).

$\theta_{el}$ elastic Debye temperature, between (15) and (16).

$\theta_{cal}(T)$ calorimetric Debye temperature, between (15) and (16).

$\theta_{cal}(0)$ low-temperature limit of $\theta_{cal}(T)$.

$\theta_{cal}(\infty)$ high-temperature limit of $\theta_{cal}(T)$.

$\theta, \phi$ direction angles, (A1).

$\mu(x, t)$ displacement of a point at $x$ in the crystal as a function of time $t$, between (2) and (3).

$\xi_1$ amplitude of motion of heavy particles, (25b).

$\xi_2$ amplitude of motion of light particles, (25a).

$\pi$ constant, equal to 3.14159.

$\sigma_P$ Poisson's ratio, between (15) and (16).

$\phi_j$ force constant between two atoms (on one-dimensional chain) separated from each other by $j$ lattice constants, (16).

$\phi_1$ nearest-neighbor force constant, (19).

$\phi_1, \phi_2$ force constants in a diatomic chain, (24a).

$\omega$ angular frequency, radians per second, (3).

$\omega_D$ Debye cutoff frequency, (9).

$\omega_D'$ cutoff frequency of truncated Debye spectrum, (32).

$\omega_E$ Einstein frequency, after (40).

$\omega_m$ maximum lattice frequency of a lattice of discrete points, (21).

$\omega_0$ frequency of vibration of diatomic chain at Brillouin zone center, acoustic branch, (2/a).

$\omega_1$ frequency of vibration of diatomic chain at Brillouin zone center, optic branch, (27b).

$\omega_2$ frequency of vibration of diatomic chain at Brillouin zone boundary, acoustic branch, (28a).

$\omega_3$ frequency of vibration of diatomic chain at Brillouin zone boundary, optic branch, (28b).

$\Omega$ solid angle, (7).

## REFERENCES

Alers, G. A., Use of sound velocity measurements in determining the Debye temperature of solids, in *Physical Acoustics*, edited by W. P. Mason, pp. 1–42, Academic, New York, 1965.

Alexandrov, K. S., and T. V. Ryzhova, Elastic properties of rock-forming minerals, III, Feldspars, *Bull. Acad. Sci. USSR Geophys. Ser.*, Engl. Transl., 2, 129–131, 1962.

Alexandrov, K. S., T. V. Ryzhova, and B. P. Belikov, The elastic properties of pyroxenes, *Sov. Phys. Crystallogr.*, 8, 589–591, 1964.

Anderson, C. T., The heat capacities at low temperatures of the alkaline earth carbonates, *J. Amer. Chem. Soc.*, 56, 340–342, 1934.

Anderson, C. T., The heat capacities of quartz, cristobalite and tridymite at low temperatures, *J. Amer. Chem. Soc.*, 58, 568–570, 1936.

Anderson, O. L., A simplified method for calculating the Debye temperature from elastic constants, *J. Phys. Chem. Solids*, 24, 909–917, 1963.

Anderson, O. L., and R. C. Liebermann, Sound velocities in rocks and minerals, *Contract Rep. 7885-4-X*, Willow Run Lab., Ann Arbor, Mich., 1966.

Barron, T. H. K., and J. A. Morrison, The thermal properties of alkali halide crystals, III, The inversion of the heat capacity. *Proc. Roy. Soc. London, Ser., A*, 256, 427–439, 1957.

Barron, T. H. K., W. T. Berg, and J. A. Morrison, On the heat capacity of crystalline magnesium oxide, *Proc. Roy. Soc. London, Ser., A*, 250, 70–83, 1959.

Bernstein, B. T., Elastic constants of synthetic sapphire at 27°C, *J. Appl. Phys.*, 34(1), 169–172, 1963.

Bhatia, A. B., and G. K. Horton, Vibration spectra and specific heats of cubic metals, II, Application to silver, *Phys. Rev.*, 98, 1715–1721, 1955.

Blackman, M., The specific heat of solids, in *Handbuch der Physik*, vol. 7, part 1, pp. 325–382, Springer, New York, 1955.

Blanchard, R., and Y. P. Varshni, Lattice dynamics of diamond, *Phys. Rev.*, 159, 599–602, 1967.

Bonnickson, K. R., High temperature heat contents of aluminates of calcium and magnesium, *J. Phys. Chem.*, 59, 220–221, 1955.

Borgonovi, G. M., and G. W. Carriveau, Neutron scattering from MgO, *Phys. Rev.*, 174, 953–958, 1968.

Born, M., and K. Huang, *Dynamical Theory of Crystal Lattices*, 420 pp., Oxford University Press, New York, 1954.

Born, M., and T. von Karman, Über Schwingungen in Raumgittern, *Phys. Z.*, 13, 297–309, 1912.

Born, M., and T. von Karman, Theory of specific heat, *Phys. Z.*, 14, 15–71, 1913.

Brillouin, L., *Wave Propagation in Periodic Structures*, 255 pp., Dover, New York, 1953.

Cetas, T. C., C. R. Tilford, and C. A. Swenson, Specific heats of Cu, GaAs, GaSb, InAs, and InSb from 1 to 30°K, *Phys. Rev.*, 174, 835–844, 1968.

Clusius, K., J. Goldmann, and A. Perlick, Ergebnisse der Treftemperaturforschung, *Z. Naturforsch.*, A4, 424–432, 1949.

Debye, P., Zur Theorie der spezifischen Wärmen, *Ann. Phys. Leipzig*, 39, 789–839, 1912. (Translation in *The Collected Papers of Peter J. W. Debye*, Interscience, New York, 1954.)

Donovan, B., and J. F. Angress, *Lattice Vibrations*, 190 pp., Chapman and Hall, London, 1971.

Dugdale, J. S.. J. A. Morrison, and D. Patterson, The effect of particle size on the heat capacity of titanium dioxide, *Proc. Roy. Soc. London, Ser. A, 224*, 228–235, 1954.

Elcombe, M. H., Some aspects of the lattice dynamics of quartz, *Proc. Phys. Soc. London, 91*, 947–958, 1967.

Flubacher, P., A. J. Leadbetter, J. A. Morrison, and B. P. Stoicheff, The low-temperature heat capacity and the Raman and Brillouin spectra of vitreous silica, *J. Phys. Chem. Solids, 12*, 53–65, 1959.

Giauque, W. F., and R. C. Archibald, The entropy of water from the third law of thermodynamics: The dissociation pressure and calorimetric heat of the reaction $Mg(OH)_2 = MgO + H_2O$: The heat capacities of $Mg(OH)_2$ and MgO from 20 to 300°K, *J. Amer. Chem. Soc., 59*, 561–569, 1937.

Ginnings, D. C., and G. T. Furukawa, Heat capacity standards for the range 14 to 1200°K, *J. Amer. Chem. Soc., 75*, 522–527, 1953.

Gopal, E. S. R., *Specific Heats at Low Temperatures*, Plenum, New York, 1966.

Hill, R. W., and D. H. Parkinson, The specific heats of germanium and grey tin at low temperatures, *Phil. Mag., 43*, 309–316, 1952.

Holm, J. L., O. L. Kleppa, and E. F. Westrum, Jr., Thermodynamics of polymorphic transformations in silica: Thermal properties from 5 to 1070°K and pressure-temperature stability fields for coesite and stishovite, *Geochim. Cosmochim. Acta, 31*, 2289–2307, 1967.

Horton, G. K., and H. Schiff, Low temperature behavior and dispersion relations of face-centered cubic metals, *Phys. Rev., 104*, 32–36, 1956.

Janaff, Thermochemical tables, Joint Army, Navy, and Air Force Project Principia of the Advanced Research Projects Agency, *Rep. PB 168 370*, Therm. Res. Lab., Dow Chem. Co., Midland, Mich., 1965a. (Also available from Clearinghouse, U.S. Dep. of Commer., Springfield, Va.)

Janaff, Thermochemical tables, first addendum, Joint Army, Navy, and Air Force Project Principia of the Advanced Research Projects Agency, Therm. Res. Lab., Dow Chem. Co., Midland, Mich., 1965b.

Janaff, Thermochemical tables, second addendum, Joint Army, Navy, and Air Force Project Principia of the Advanced Research Projects Agency, Therm. Res. Lab., Dow Chem. Co., Midland, Mich., 1966.

Janaff, Thermochemical tables, third addendum, Joint Army, Navy, and Air Force Project Principia of the Advanced Research Projects Agency, Therm. Res. Lab., Dow Chem. Co., Midland, Mich., 1967.

Karo, A. M., and J. R. Hardy, Lattice dynamics and specific heat data of CsCl, CsBr, and CsI, *J. Chem. Phys., 48*, 3173–3184, 1968.

Katz, E., Note on frequency spectra of simple solids from specific heat data, *J. Chem. Phys., 19*, 488–493, 1951.

Keesom, P. H., and N. Pearlman, Low temperature heat capacity of pure and reduced rutile, *Phys. Rev., 112*, 800–804, 1958.

Kelley, K. K., The specific heats at low temperatures of ferrous silicate, manganous silicate and zirconium silicate, *J. Amer. Chem. Soc., 63*, 2750–2752, 1941.

Kelley, K. K., Specific heats at low temperatures of magnesium orthosilicate and magnesium metasilicate, *J. Amer. Chem. Soc., 65*, 339–341, 1943.

Kelley, K. K., Contributions to the data on theoretical metallurgy, XIII, High-temperature heat-content, heat-capacity, and entropy data for the elements and inorganic compounds, *U.S. Bur. Mines Bull., 584*, 1960.

Kelley, K. K., S. S. Todd, R. L. Orr, E. G. King, and K. R. Bonnickson, Thermal properties of sodium-aluminum and potassium-aluminum silicates, *U.S. Bur. Mines Rep. Invest., 4955*, 1953.

Kieffer, S. W., What can vibrational spectroscopy tell us about the thermodynamic properties of minerals?, *Amer. Mineral.*, in press, 1979a.

Kieffer, S. W., Thermodynamics and lattice vibrations of minerals, 2, Vibrational characteristics of silicates, *Rev. Geophys. Space Phys., 17*, this issue, 1979b.

Kieffer, S. W., Thermodynamics and lattice vibrations of minerals, 3, Lattice dynamics and an approximation for minerals with applications to simple substances and framework silicates, *Rev. Geophys. Space Phys., 17*, this issue, 1979c.

King, E. G., Heat capacities at low temperatures and entropies at 298.16°K of crystalline calcium and magnesium aluminates, *J. Phys. Chem., 59*, 218–219, 1955.

King, E. G., Low temperature heat capacities and entropies at 298.15°K of some crystalline silicates containing calcium, *J. Amer. Chem. Soc., 79*, 5437–5438, 1957.

Kiseleva, I. A., N. D. Topor, and L. V. Melchakova, Experimental determination of the heat content and heat capacity of grossular, andradite and pyrope (in Russian), *Geokhimiya, 11*, 1372–1379, 1972.

Kittel, C., *Introduction to Solid State Physics*, 3rd ed., 648 pp., John Wiley, New York, 1968.

Kumazawa, M., The elastic constants of single-crystal orthopyroxene, *J. Geophys. Res., 74*, 5973–5980, 1969.

Launer, P. J., Regularities in the infrared absorption spectra of silicate minerals, *Amer. Mineral., 37*, 764–784, 1952.

Lazarev, A. N., Vibrational spectra and structure of silicates, translated from Russian, 302 pp., Consultants Bureau, New York, 1972.

Leibfried, G., Gittertheorie der mechanischen und thermischen Ergenschaften der Kristalle, in *Handbuch der Physik*, vol. 7, part 1, pp. 104–324, Springer, New York, 1955.

Lewis, M. F., Elastic constants of magnesium aluminate spinel, *J. Acoust. Soc. Amer., 40*, 728–729, 1966.

Lord, R. C., The heat capacities of molecular lattices, *J. Chem. Phys., 9*, 693–699, 1941.

Lord, R. C., and J. C. Morrow, Calculation of the heat capacity of $\alpha$-quartz and vitreous silica from spectroscopic data, *J. Chem. Phys., 26*, 230–232, 1957.

Manghnani, M., Elastic constants of single-crystal rutile under pressures to 7.5 kbar, *J. Geophys. Res., 74*, 4317–4328, 1969.

Maradudin, A. A., E. W. Montroll, and G. H. Weiss, *Lattice Dynamics in the Harmonic Approximation*, Academic, New York, 1963.

McSkimmin, H. J., P. Andreatch, Jr., and R. N. Thurston, Elastic moduli of quartz versus hydrostatic pressure at 25° and −195.8°C, *J. Appl. Phys., 36*, 1624–1632, 1965.

Moenke, H. H. W., Vibrational spectra and the crystal-chemical classification of minerals, in *The Infrared Spectra of Minerals, Monogr. 4*, edited by V. C. Farmer, pp. 111–118, Mineralogical Society, London, 1974.

Openshaw, R., The low-temperature heat capacities of analbite, low-albite, microcline and sanidine, Ph.D. thesis, 312 pp., Princeton Univ., Princeton, N. J., 1974.

Orr, R. L., High-temperature heat contents of magnesium orthosilicate and ferrous orthosilicate, *J. Amer. Chem. Soc., 75*, 528–529, 1953.

Pandey, H. N., The theoretical elastic constants and specific heats of rutile, *Phys. Status Solidi, 11*, 743–751, 1965.

Pesselnick, L., and R. A. Robie, Elastic constants of calcite, *J. Appl. Phys., 34*(8), 2494–2495, 1963.

Reif, F., *Fundamentals of Statistical and Thermal Physics*, 651 pp., McGraw-Hill, New York, 1965.

Robie, R. A., and J. L. Edwards, Some Debye temperatures from single-crystal elastic constant data, *J. Appl. Phys., 37*, 2659–2663, 1966.

Ryzhova, T. V., Elastic properties of plagioclase, *Izv. Acad. Sci. USSR Geophys. Ser.*, Engl. Transl., 7, 1049–1051, 1964.

Ryzhova, T. V., K. S. Alexandrov, and V. M. Korobkova, The elastic properties of rock-forming minerals, V, Additional data on silicates, *Izv. Acad. Sci. USSR Phys. Solid Earth*, Engl. Transl., 2, 111–113, 1966.

Sandin, T. R., and P. H. Keesom, Specific heat and paramagnetic susceptibility of stoichiometric and reduced rutile ($TiO_2$) from 0.3 to 20°K, *Phys. Rev., 177*, 1370–1383, 1969.

Shomate, C. H., Heat capacities at low temperatures of titanium dioxide, *J. Amer. Chem. Soc., 69*, 218–219, 1947.

Simmons, G., and H. Wang, *Single Crystal Elastic Constants and Calculated Aggregate Properties: A Handbook*, 2nd ed., 370 pp., MIT Press, Cambridge, Mass., 1971.

Simon, F., and W. Zeidler, Untersuchungen über die spezifischen Wärmen bei teifen Temperature, *Z. Phys. Chem., 123*, 383–405, 1926.

Spetzler, H., Equation of state of polycrystalline MgO and single crystal MgO to 8 kbar and 800°K, *J. Geophys. Res., 75*, 2073–2087, 1970.

Stavely, L. A. K., and R. G. Linford, The heat capacity and entropy of calcite and aragonite, and their interpretation, *J. Chem. Thermodyn., 1*, 1–11, 1969.

Thomsen, L., Elasticity of polycrystals and rocks, *J. Geophys. Res., 77*, 315–327, 1972.

Todd, S. S., Heat capacities at low temperatures and entropies at 298.16°K of andalusite, kyanite and sillimanite, *J. Amer. Chem. Soc., 72*, 4742–4743, 1950.

Traylor, J. G., H. G. Smith, R. M. Nicklow, and M. K. Wilkinson, Lattice dynamics of rutile, *Phys. Rev. B, 3*(10), 3457–3472, 1971.

Verma, R. K., Elasticity of some high-density crystals, *J. Geophys. Res., 65*, 757–766, 1960.

Weidner, D. J., and H. R. Carleton, Elasticity of coesite, *J. Geophys. Res., 82*, 1334–1346, 1977.

White, W. B., Structural interpretation of lunar and terrestrial minerals by Raman spectroscopy, in *Infrared and Raman Spectroscopy of Lunar and Terrestrial Minerals,* edited by C. Karr, Jr., pp. 325–358, Academic, New York, 1975.

Ziman, J. M., *Principles of the Theory of Solids,* 2nd ed., 435 pp., Cambridge University Press, New York, 1972.